

# Localization from semantic observations via the matrix permanent

The International Journal of  
Robotics Research  
2016, Vol. 35(1–3) 73–99  
© The Author(s) 2015  
Reprints and permissions:  
[sagepub.co.uk/journalsPermissions.nav](http://sagepub.co.uk/journalsPermissions.nav)  
DOI: 10.1177/0278364915596589  
[ijr.sagepub.com](http://ijr.sagepub.com)  


Nikolay Atanasov, Menglong Zhu, Kostas Daniilidis and George J. Pappas

## Abstract

*Most approaches to robot localization rely on low-level geometric features such as points, lines, and planes. In this paper, we use object recognition to obtain semantic information from the robot's sensors and consider the task of localizing the robot within a prior map of landmarks, which are annotated with semantic labels. As object recognition algorithms miss detections and produce false alarms, correct data association between the detections and the landmarks on the map is central to the semantic localization problem. Instead of the traditional vector-based representation, we propose a sensor model, which encodes the semantic observations via random finite sets and enables a unified treatment of missed detections, false alarms, and data association. Our second contribution is to reduce the problem of computing the likelihood of a set-valued observation to the problem of computing a matrix permanent. It is this crucial transformation that allows us to solve the semantic localization problem with a polynomial-time approximation to the set-based Bayes filter. Finally, we address the active semantic localization problem, in which the observer's trajectory is planned in order to improve the accuracy and efficiency of the localization process. The performance of our approach is demonstrated in simulation and in real environments using deformable-part-model-based object detectors. Robust global localization from semantic observations is demonstrated for a mobile robot, for the Project Tango phone, and on the KITTI visual odometry dataset. Comparisons are made with the traditional lidar-based geometric Monte Carlo localization.*

## Keywords

Active semantic localization, Monte Carlo localization, mobile robot localization, matrix permanent, random finite set, particle filter, conditional entropy, object recognition, deformable part model, Project Tango

## 1. Introduction

Localization, the problem of estimating the pose of a mobile robot from sensor data given a prior map, is fundamental in the field of robotics. Reliable navigation, object manipulation, mapping, and many other tasks require accurate knowledge of the robot's pose. Most existing approaches to localization and the related simultaneous localization and mapping (SLAM) rely on low-level geometric features such as points, lines, and planes. In contrast, we propose to use the recent advances in object recognition to obtain semantic information from the robot's sensors and localize the robot within a prior map of landmarks, which are annotated with semantic labels. Our approach is not meant to replace, but rather enhance, the existing localization and SLAM solutions. It offers several benefits. Localizing against semantically-meaningful landmarks is less ambiguous and can be used for global localization and loop-closure. Also, high-precision sensors such as laser rangefinders and 3-D lidars are not crucial for accurate localization and can be replaced by regular

cameras. Finally, semantically annotated maps can be constructed for GPS-denied environments via the mapping approaches that received significant attention in recent years (Civera et al., 2011; Galindo et al., 2005; Kostavelis and Gasteratos, 2013; Nüchter and Hertzberg, 2008; Pronobis, 2011).

A preliminary version of this paper appeared at the 2014 Robotics: Science and Systems Conference (Atanasov et al., 2014). This version extends and clarifies the theoretical results regarding semantic localization, addresses the active semantic localization problem, and provides additional real-world experiments, which demonstrate global localization for the Project Tango phone (Google ATAP

---

GRASP Laboratory, University of Pennsylvania, Philadelphia, PA, USA

### Corresponding author:

Nikolay Atanasov, GRASP Laboratory, University of Pennsylvania, Philadelphia, PA 19104, USA.  
Email: [atanasov@seas.upenn.edu](mailto:atanasov@seas.upenn.edu)

group, 2014) and on the KITTI visual odometry dataset (Geiger et al., 2013).

### 1.1. Related work

Monte Carlo localization based on geometric features was proposed by Dellaert et al. (1999). The knowledge about the robot pose is represented by a weighted set of samples (particles) and is updated over time as the robot moves and senses the environment. This and other traditional localization methods use vectors to represent the map and the sensor measurements. Bayesian filtering in the resulting vector space relies on the assumption that the *data association*, i.e. the correspondence between the sensor observations and the features on the map, is known. While this might not be an issue for scan matching in occupancy-grid maps, the assumption is violated for landmark-based maps. Existing landmark-based localization and SLAM techniques require external solutions to the problems of data association and clutter rejection (Bailey, 2002; Montemerlo and Thrun, 2003). Moreover, state-of-the-art approaches nowadays are based on factor graphs (Kaess et al., 2008; Kummerle et al., 2011) and rely heavily on continuous Gaussian random variables. The introduction of semantic labels for the landmarks is not addressed in existing work and requires handling discrete (non-Gaussian) variables in the estimation.

There is a line of work addressing visual localization, which matches observed image features to an image database, whose images correspond to the nodes of a topological map (Angeli et al., 2009; Košecká and Li, 2004; Mariottini and Roumeliotis, 2011; Se et al., 2005; Wang et al., 2006; Wolf et al., 2005). Wang et al. (2006) represent each location in the topological map by a set of interest points that can be reliably detected in images and use nearest neighbor search to match observed scale-invariant feature transform (SIFT) features to the database. Košecká and Li (2004) also characterize scale-invariant key points by the SIFT descriptor and find nodes in the topological map, whose features match the observed ones the best. The drawback of this most likely data association approach is that when it is wrong it quickly causes the estimation procedure to diverge. Hesch et al. (2013) study the effects of unobservable directions on the estimator consistency in vision-aided inertial navigation systems. In the SLAM context, bad data association can be mitigated by a two-stage approach, in which the back-end (e.g. factor graph) optimizer is allowed to reject or alter associations proposed by the front-end (e.g. appearance-based place recognition) (Sünderhauf and Protzel, 2011). As object recognition algorithms miss detections and produce false alarms, correct data association is crucial for semantic localization and semantic world modeling too (Wong et al., 2013).

Instead of the traditional vector-based representation, we use random finite sets to model the semantic information obtained from object recognition. This allows us to explicitly incorporate missed detections, false alarms, and data association in the sensor model. In recent years, random-

finite-set-based solutions to SLAM have gained popularity due to their unified treatment of filtering and data association. Mahler (2007) derived the Bayesian recursion with random-finite-set-valued observations and proposed a first-moment approximation, called the probability hypothesis density (PHD) filter. The PHD filter has been successfully applied to SLAM by Kalyan et al. (2010), Lee et al. (2013), and Mullane et al. (2011). In these works, the vehicle trajectory is tracked by a particle filter and the first moment of a trajectory-conditioned map for each particle is propagated via a Gaussian-mixture PHD filter. Bishop and Jensfelt (2010) address global geometric localization by formulating hypotheses about the robot state and tracking them with the PHD filter. Zhang et al. (2012) propose an approach for visual odometry using a PHD filter to track SIFT features extracted from observed images. Most of the random-set approaches rely on a first-moment approximation via the PHD filter. Only few deal with the full observation model (Dames et al., 2013; Ma et al., 2006; Sidenbladh and Wirkander, 2003) and none have applied the model in a semantic setting or studied its computational complexity.

There are several semantic localization approaches that do not rely on a random-finite-set model. Anati et al. (2012) match histogram-of-gradient-energies and quantized-colors features to the expected features from a prior semantic map. Yi et al. (2009) and Ko et al. (2013) use semantic descriptions of distance and bearing in a contextual map for active semantic localization. Bao and Savarese (2011) propose a maximum-likelihood-estimation formulation for semantic structure from motion. In addition to recovering camera parameters (motion) and 3-D locations of image features (structure), the authors recover the 3-D locations, orientations, and categories of objects in the scene. A Markov chain Monte Carlo algorithm is used to solve a batch estimation problem by sampling from the data likelihood of the observed measurements.

### 1.2. Summary of contributions

We make the following contributions.

- We represent the semantic information obtained from object recognition with random finite sets. This allows a unified treatment of missed detections, false alarms, and data association in the sensor model.
- We prove that obtaining the likelihood of a set-valued observation is equivalent to a matrix permanent computation. It is this crucial transformation that enables an efficient polynomial-time approximation to Bayesian filtering with set-valued observations.
- We address the active semantic localization problem, in which the observer's trajectory is planned in order to minimize the entropy of the pose distribution, conditioned on the future measurements.

Connections between the matrix permanent and data association have been identified in the target tracking

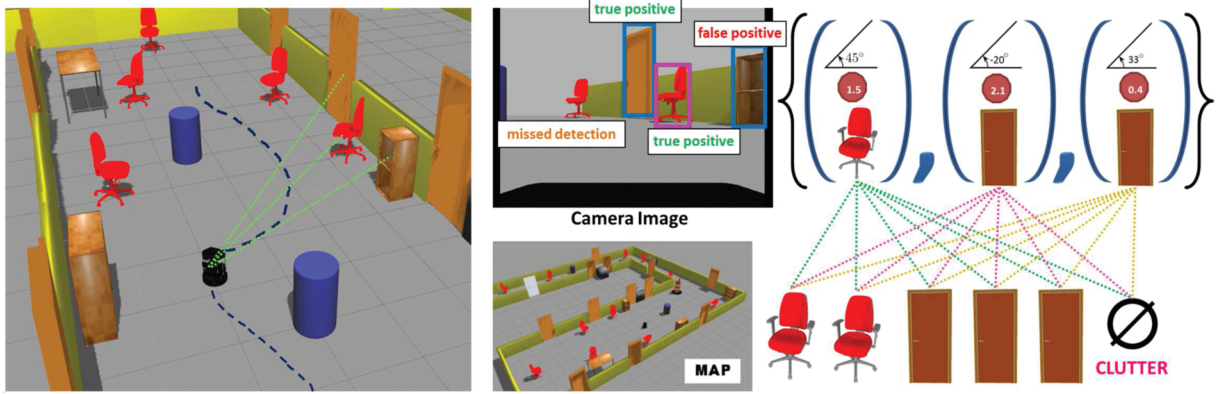


**Fig. 1.** A mobile robot (left) localizes itself within a semantic map of the environment by detecting chairs and doors in images (top middle), obtained from its surroundings. A semantic observation received by the robot (top right) consists of a detected class, a detection (confidence) score, and a bearing angle to the detected bounding box. Due to the fact that object recognition misses detections (only one of the two visible chairs is detected) and produces false positives (there is an incorrect door detection), it is appropriate to model the collection of semantic observations via a *set with randomly-varying cardinality*. Finally, correct data association between the object detections (top right) and the landmarks on the prior map (bottom right) plays a key role in the robot’s ability to estimate its location.

community (Collins and Uhlmann, 1992; Liggins et al., 2008, ch. 11; Morelande, 2009; Oh et al., 2009; Pasula et al., 1999) but this is the first connection with the random-finite-set observation model.

### 1.3. Paper organization

In Section 2 we formulate the semantic localization problem precisely. In Section 3 we provide a probabilistic model, which quantifies the likelihood of a random finite set of semantic observations and captures false positives, missed detections, and unknown data association. The key relationship between filtering with the random-finite-set observation model and the matrix permanent is derived in Section 4. In Section 5, we introduce the active semantic localization problem and discuss the efficient minimization of the observer’s pose entropy conditioned on the future semantic measurements. Finally, in Section 6, we present results from simulations and real-world experiments and discuss the performance of our approach.

## 2. Problem formulation

Consider a mobile robot, whose dynamics are governed by the *motion model*  $x_{t+1} = f(x_t, u_t, v_t)$ , where  $x_t := (x_t^p, x_t^r, x_t^a)$  is the robot state, containing its position  $x_t^p$ , orientation  $x_t^r$ , and other variables  $x_t^a$ , such as velocity and acceleration,  $u_t$  is the control input, and  $v_t$  is the motion noise. Alternatively, the model can be specified by the probability density function (pdf) of  $x_{t+1}$  conditioned on  $x_t$  and  $u_t$ :

$$p_f(\cdot | x_t, u_t) \quad (1)$$

The robot has access to a semantic map of the environment, containing  $n$  objects with known poses and classes. Let the set  $Y = \{y_1, \dots, y_L\}$  represent the map, where

$y_i := (y_i^p, y_i^r, y_i^c)$  consists of the position  $y_i^p$ , orientation  $y_i^r$ , and class  $y_i^c$  of the  $i$ th object. Depending on the application, the object state  $y_i$  may capture other observable properties of interest, such as shape priors (Dame et al., 2013).

At each time  $t$ , the robot receives data from its sensors and runs an object recognition algorithm, capable of detecting instances from the set of object classes  $\mathcal{C}$ , present in  $Y$ . If some object  $y \in Y$  is visible and detected from the current robot pose  $x_t$ , then a semantic measurement  $z_t$  is obtained. In the remainder, we assume that a semantic measurement,  $z_t := (c_t, s_t, b_t)$ , consists of a detected class  $c_t \in \mathcal{C}$ , a detection score  $s_t \in \mathcal{S}$ , and an estimate  $b_t \in \mathcal{B}$  of the bearing from the sensor to the detected object, where  $\mathcal{S}$  is the range of possible scores and  $\mathcal{B}$  is the range of bearings, usually specified by the sensor’s field of view (e.g. a camera with  $\mathcal{B} = [-47^\circ, 47^\circ]$  was used in our experiments). Depending on the sensors and the visual processing,  $z_t$  could also contain bounding box, range, color, or other information about the detected object. Detections might also be generated by clutter, which includes the background and any objects not captured on the map  $Y$ . Figure 1 illustrates the object recognition process and the challenges associated with it. Due to false alarms and missed detections, a randomly sized collection of measurements is received at time  $t$ . Instead of the traditional vector representation, it is more appropriate to model the collection of semantic observations via a random finite set<sup>2</sup>  $Z_t$ . For any  $t$ , denote the pdf of robot state  $x_t$  conditioned on the map  $Y$ , the past semantic observations  $Z_{0:t}$ , and the control history  $u_{0:t-1}$  by  $p_{t|t}$  and that of  $x_{t+1}|Y, Z_{0:t}, u_{0:t}$  by  $p_{t+1|t}$ .

**Problem 1** (Semantic localization). *Suppose that control  $u_t$  is applied at time  $t \geq 0$  and, after moving, the robot obtains a random finite set  $Z_{t+1}$  of semantic observations. Given a prior pdf  $p_{t|t}$  and the semantic map  $Y$ , compute the posterior pdf  $p_{t+1|t+1}$  which takes  $Z_{t+1}$  and  $u_t$  into account.*

### 3. Semantic observation model

It is natural to approach the semantic localization problem via recursive Bayesian estimation. This, however, requires a probabilistic model, which quantifies the likelihood of a random set  $Z_{t+1}$  of semantic observations, conditioned on the set of objects  $Y$  and the robot state  $x_{t+1}$ . Really, the first challenge of the semantic localization problem is a modeling one. In Section 3.1, we model the likelihood of an observation received from a single object in the environment. Then, in Section 3.2, we combine the single-object observation models into an observation model for multiple objects, which captures data association, missed detections, and false alarms.

#### 3.1. Observation model for a single object

The probabilistic model of a semantic observation obtained from a single object consists of three ingredients: a *detection model*, an *observation likelihood*, and a *clutter model*.

The detection model quantifies the probability of detecting an object  $y \in Y$  from a given robot state  $x$ . Let  $\beta(x, y)$  be the true bearing angle from the robot's sensor to the object  $y$  in the sensor frame.<sup>3</sup> Let the field of view of the sensor be described by the set  $FoV(x)$ . Objects outside the field of view cannot be detected. For the ones within, we use a distance-decaying probability of detection:

$$p_d(y, x) := \begin{cases} p_0 \exp\left\{-\frac{|m_0 - \|y^p - x^p\|_2|}{v_0}\right\} & \text{if } y^p \in FoV(x) \\ 0 & \text{otherwise} \end{cases} \quad (2)$$

where  $p_0$ ,  $m_0$ ,  $v_0$  are constants specifying the dependence of the detection probability on distance and are typically learned from training data. The constants might depend on the object's class  $y^c$  but this is not explicit to simplify notation. A more complex model which depends on the relative orientation between  $x$  and  $y$  or uses a different function of the distance is also possible. Figure 2 illustrates the detection model. If visibility information is available from the prior map, it should also be considered when calculating the probability of detection.

When an object  $y \in Y$  is detected, the probability of the resulting measurement  $z = (c, s, b)$  is quantified by the observation likelihood. Assuming that conditioned on the true object state  $y$ , the bearing measurement  $b$  is independent of the class  $c$  and score  $s$  measurements, it is appropriate to model its conditional pdf  $p_\beta(\cdot | y, x)$  as that of a truncated Gaussian distribution over the bearing range  $\mathcal{B}$  with mean  $\beta(x, y)$  and covariance  $\Sigma_\beta$ . The covariance can be learned from training data and can be class dependent. Since object recognition algorithms aim to be scale- and orientation-invariant, we can also assume that the class and score measurements are independent of the robot state  $x$ .

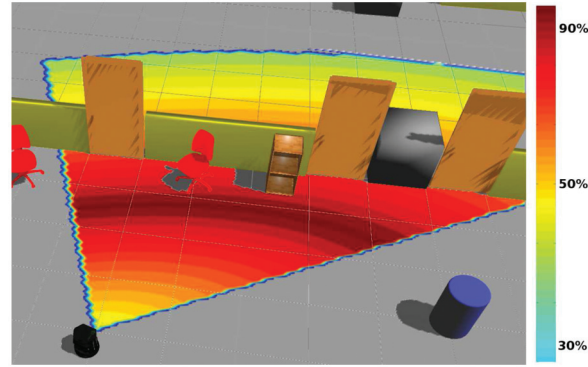


**Fig. 2.** Probability of detecting an object within the sensor field of view (without accounting for visibility).

Then, the observation likelihood of a semantic measurement  $z$  can be decomposed as

$$p_z(z | y, x) := p_c(c | y^c) p_s(s | c, y^c) p_\beta(b | y, x) \quad (3)$$

where  $p_c(c | y^c)$  is the confusion matrix of the object detector and  $p_s(s | c, y^c)$  is a score likelihood. The latter can be learned, for example, by recording the scores from the detected positive examples in a training set and using kernel density estimation (see Figure 16). A more complicated generative model can be used to approximate the observation likelihood  $p_z$ . For example, FAB-Map (Cummins and Newman, 2008) uses a Chow Liu tree to approximate a probability distribution over visual words learned from speeded-up robust features (SURF) descriptors.

Finally, a model of the pdf,  $p_\kappa(z)$ , of a false-positive measurement generated by clutter is needed. For example, FAB-Map (Cummins and Newman, 2008) models the probability that an observation is generated from a place not in the prior map. In our case,  $p_\kappa(z)$  is a product of three terms as in (3) but it is realistic to assume that the bearing measurement is independent of the robot state and uniformly distributed, i.e. with pdf  $1/|\mathcal{B}|$ . The class and score likelihoods should be learned from data.

#### 3.2. Observation model for multiple objects

In this section, we combine the single-object observation models into a model of the likelihood of a set  $Z = \{z_1, \dots, z_m\}$  of semantic observations. Given a robot pose  $x$ , let  $Y_d(x) := \{y \in Y \mid p_d(y, x) > 0\}$  be the set of objects, detectable from  $x$ . In the reminder, we denote the cardinality of  $Z$  by  $m$  and that of  $Y_d(x)$  by  $n$ . As mentioned earlier, the data association  $\pi$  between the semantic observations in  $Z$  and the visible objects in  $Y_d(x)$  is important for constructing the multi-object observation model. The following assumptions are necessary:

- (A1) no measurement is generated by more than one object;
- (A2) an object  $y \in Y$  generates either a single detection with probability  $p_d(y, x)$  in (2) or a missed detection with probability  $1 - p_d(y, x)$ ;
- (A3) the process of receiving false-positive measurements is Poisson-distributed in time with expected value  $\lambda$  and distributed in space according to the pdf  $p_\kappa(z)$ ;
- (A4) the false-positive process and the object-detection process are independent and all detections are conditionally independent given the robot and object states;
- (A5) any two measurements in  $Z$  are independent conditioned on the robot state  $x$ , the detectable objects  $Y_d(x)$ , and the data association  $\pi$ .

We specify the pdf of  $Z$ , conditioned on  $x$  and  $Y_d(x)$ , in five steps of increasing complexity.

*All measurements are false positive* The simplest case is when there are no objects in proximity to the sensor, i.e.  $Y_d(x) = \emptyset$ . Then, any generated measurements would be from clutter. The correct observation model in this case is due to assumption (A3) of a Poisson false-positive process:

$$p(Z|\emptyset, x) = \frac{e^{-\lambda} \lambda^{|Z|}}{|Z|!} \prod_{z \in Z} p_\kappa(z) \quad (4)$$

This integrates to 1 if we use the set integral definition in Mahler (2007: Ch.11.3.3):

$$\int p(Z) dZ := \sum_{m=0}^{\infty} \int p(\{z_1, \dots, z_m\}) dz_1 \dots dz_m$$

*No missed detections and no false positives* Next, suppose that there are detectable objects in proximity to the sensor but let the detection be perfect. In other words, assume that every detectable object generates a measurement, i.e.  $p_d(y, x) = 1$  for any  $y \in FoV(x)$ , and no measurements arise in any other way, i.e.  $\lambda = 0$ . If the number of measurements  $m$  is not equal to the cardinality  $n$  of the set of detectable objects  $Y_d(x)$ , then  $p(Z|Y_d(x), x) = 0$ . Otherwise, the main challenge in this “perfect detection” case is identifying the correct data association  $\pi$ . In other words, it is not clear which of the detectable objects  $Y_d(x)$  on the map produced which of the measurements in  $Z$ .

More formally, let  $\Pi_{n,m}$  be the set of *one-to-one* functions  $g : \{1, \dots, n\} \rightarrow \{1, \dots, m\}$  with  $n \leq m$ . Due to the “perfect detection” assumption  $m = n$  and a particular data association can be represented by a mapping  $\pi \in \Pi_{n,n}$  from the set of detectable objects to the set of measurements. In this case, the data association  $\pi$  is just a permutation of  $\{1, \dots, n\}$  but it is not clear which of the possible  $|\Pi_{n,n}| = n!$  associations is the correct one.

If a particular data association  $\pi$  is chosen, it is straightforward to combine the single-object observation likelihoods in (3) via the independence assumptions (A4), (A5) to obtain the pdf of  $Z$ :

$$p(Z|Y_d(x), x, \pi) = \prod_{i=1}^n p_z(z_{\pi(i)}|y_i, x)$$

where  $\{y_1, \dots, y_n\}$  is an enumeration of  $Y_d(x)$ . Assuming a uniform prior on the possible data associations:

$$p(\pi|Y_d(x), x) = \frac{1}{n!}, \quad \pi \in \Pi_{n,n}$$

existing work (e.g. FastSLAM by Montemerlo and Thrun (2003)) resorts to maximum-likelihood estimation and computes the likelihood of  $Z$  as follows:

$$p(Z|Y_d(x), x) \stackrel{?}{=} \frac{1}{n!} \max_{\pi \in \Pi_{n,n}} \left( \prod_{i=1}^n p_z(z_{\pi(i)}|y_i, x) \right)$$

The above equality, however, disagrees with the law of total probability, which states that the data association should be marginalized. The observation model in the “perfect detection” case is

$$\begin{aligned} p(Z|Y_d(x), x) &= \sum_{\pi \in \Pi_{n,n}} p(Z|Y_d(x), x, \pi) p(\pi|Y_d(x), x) \\ &= \frac{1}{n!} \sum_{\pi \in \Pi_{n,n}} \prod_{i=1}^n p_z(z_{\pi(i)}|y_i, x) \end{aligned} \quad (5)$$

Intuitively, all associations are plausible and (5) is quantifying the likelihood of  $Z$  by averaging the likelihoods of the individual measurements over all possible data associations. The reason, why existing work avoids this marginalization, is that the summation over all  $n!$  data associations is computationally demanding. However, in Section 4, we will present an efficient method for computing (5). Before that, we relax the perfect-detection assumption.

*No false positives but missed detections are possible* Now, suppose that some of the objects in proximity to the sensor might not be detected. Assuming no false positives still, the number of measurements  $m$  should be at most the number of detectable objects  $n$ , i.e. if  $m > n$ , then  $p(Z|Y_d(x), x) = 0$ . In the case that  $m \leq n$ , we have  $\pi \in \Pi_{m,n}$  and there are  $|\Pi_{m,n}| = {}_nP_m := \frac{n!}{(n-m)!}$  possible data associations. Let  $\mathcal{D}(\pi) := \cup_{j=1}^m \{\pi(j)\}$  be the set of true-positive detections according to  $\pi$  and  $\mathcal{M}(\pi) := \{1, \dots, n\} \setminus \mathcal{D}(\pi)$  be the set of missed detections. Finally, let  $\mathcal{A}(\pi)$  be the event that the true-positive detections  $\mathcal{D}(\pi)$  are assigned to the measurements in  $Z$  in the way specified by  $\pi$ . Then, we can quantify the likelihood of  $\pi \in \Pi_{m,n}$ , using the detection model (2), as follows:

$$\begin{aligned} p(\pi|Y_d(x), x) &= \mathbb{P}(\mathcal{A}(\pi)) \\ &\times \mathbb{P}(\{\{y_i | i \in \mathcal{D}(\pi)\}\text{ are detected}\}) \\ &\times \mathbb{P}(\{\{y_i | i \in \mathcal{M}(\pi)\}\text{ are missed}\}) \\ &= \frac{1}{m!} \prod_{j=1}^m p_d(y_{\pi(j)}, x) \prod_{i \in \mathcal{M}(\pi)} (1 - p_d(y_i, x)) \end{aligned}$$

See Appendix B.2 for a verification that  $p(\pi|Y_d(x), x)$  is a valid pdf. As before, we can derive the likelihood of  $Z$  by marginalizing the data association:

$$\begin{aligned} p(Z|Y_d(x), x) &= \sum_{\pi \in \Pi_{m,n}} p(Z|Y_d(x), x, \pi)p(\pi|Y_d(x), x) \\ &= \sum_{\pi \in \Pi_{m,n}} \left[ \prod_{j=1}^m p_z(z_j|y_{\pi(j)}, x) \right] \\ &\quad \left[ \frac{1}{m!} \prod_{j=1}^m p_d(y_{\pi(j)}, x) \prod_{i \in \mathcal{M}(\pi)} (1 - p_d(y_i, x)) \right] \\ &= \frac{1}{m!} \prod_{i=1}^n (1 - p_d(y_i, x)) \\ &\quad \sum_{\pi \in \Pi_{m,n}} \prod_{j=1}^m \frac{p_d(y_{\pi(j)}, x)p_z(z_j|y_{\pi(j)}, x)}{1 - p_d(y_{\pi(j)}, x)} \end{aligned} \quad (6)$$

The observation model is similar to the “perfect detection” case in (5) but the single-object-measurement likelihoods need to be scaled by the probabilities of detection. If no measurements are received but  $Y_d(x) \neq \emptyset$ , the above simplifies to:

$$p(\emptyset|Y_d(x), x) = \prod_{i=1}^n (1 - p_d(y_i, x)) \quad (7)$$

*No missed detections but false positives are possible* In this case,  $n \leq m$  (otherwise  $p(Z|Y_d(x), x) = 0$ ) and  $\pi \in \Pi_{n,m}$ . Again, let  $\mathcal{A}(\pi)$  be the event that the true-positive detections,  $Y_d(x)$  in this case, are assigned to the measurements in  $Z$  in the particular way specified by  $\pi$ . The likelihood of  $\pi$  is

$$\begin{aligned} p(\pi|Y_d(x), x) &= \mathbb{P}(\mathcal{A}(\pi)) \times \mathbb{P}(\{n \text{ true positives}\}) \\ &\quad \times \mathbb{P}(\{m - n \text{ false positives}\}) \\ &= \frac{1}{m P_n} \times 1 \times \frac{e^{-\lambda} \lambda^{m-n}}{(m-n)!} \end{aligned}$$

which is a valid pdf (see Appendix B.3). The likelihood of  $Z$  is obtained by marginalizing the data association:

$$\begin{aligned} p(Z|Y_d(x), x) &= \sum_{\pi \in \Pi_{n,m}} p(Z|Y_d(x), x, \pi)p(\pi|Y_d(x), x) \\ &= \sum_{\pi \in \Pi_{n,m}} \prod_{i=1}^n p_z(z_{\pi(i)}|y_i, x) \\ &\quad \prod_{j \in \{1, \dots, m\} \setminus \cup_{i=1}^n \{\pi(i)\}} p_k(z_j) \frac{e^{-\lambda} \lambda^{m-n}}{m!} \\ &= \frac{e^{-\lambda} \lambda^m}{m!} \prod_{j=1}^m p_k(z_j) \sum_{\pi \in \Pi_{n,m}} \prod_{i=1}^n \frac{p_z(z_{\pi(i)}|y_i, x)}{\lambda p_k(z_{\pi(i)})} \end{aligned} \quad (8)$$

*Both missed detections and false positives are possible* Finally, consider the most general case that captures all artifacts of object recognition: missed detections, false positives, and unknown data association. If there are no detectable objects close by, i.e.  $n = 0$ , then the pdf of  $Z$  is given by (4). If no measurements are received, i.e.  $m = 0$ , then the pdf of  $Z$  is given by (7). Otherwise,  $\pi \in \bar{\Pi}_{n,m}$ , where  $\bar{\Pi}_{n,m}$  is the set of functions  $g: \{1, \dots, n\} \rightarrow \{0, 1, \dots, m\}$  with the property:  $g(i) = g(i') > 0 \Rightarrow i = i'$ , which ensures that (A1) is satisfied. The index “0” in the range of  $g$  represents the case of missing a detectable object. For example, it allows for the possibility that all detectable objects are missed (associated with “0”), in which case we obtain the term in (7). The number of possible data associations in this case is

$$|\bar{\Pi}_{n,m}| = \sum_{k=0}^{\min\{n,m\}} \binom{n}{k} m P_k$$

where the index  $k$  indicates the number of true-positive assignments made by a particular data association  $p_i$ . The likelihood of  $\pi \in \bar{\Pi}_{n,m}$  with  $k$  true-positive assignments is

$$\begin{aligned} p(\pi|Y_d(x), x) &= \mathbb{P}(\mathcal{A}(\pi)) \times \mathbb{P}(\{y_i | \pi(i) > 0\} \text{ are detected}) \\ &\quad \times \mathbb{P}(\{y_i | \pi(i) = 0\} \text{ are missed}) \\ &\quad \times \mathbb{P}(\{m - k \text{ false positives}\}) \\ &= \frac{1}{m P_k} \prod_{i: \pi(i) > 0} p_d(y_i, x) \\ &\quad \prod_{i: \pi(i) = 0} (1 - p_d(y_i, x)) \frac{e^{-\lambda} \lambda^{m-k}}{(m-k)!} \end{aligned}$$

where, as before,  $\mathcal{A}(\pi)$  is the event that the  $k$  true-positive detections are assigned to the measurements in  $Z$  in the particular way specified by  $\pi$ . See Appendix B.4 for a verification that  $p(\pi|Y_d(x), x)$  is a valid pdf. As before, we can derive the likelihood of  $Z$  by marginalizing the data association:

$$\begin{aligned} p(Z|Y_d(x), x) &= \sum_{\pi \in \bar{\Pi}_{n,m}} p(Z|Y_d(x), x, \pi)p(\pi|Y_d(x), x) \\ &= \sum_{\pi \in \bar{\Pi}_{n,m}} \left[ \prod_{i: \pi(i) > 0} p_z(z_{\pi(i)}|y_i, x) \prod_{j \in \{1, \dots, m\} \setminus \cup_{i=1}^n \{\pi(i)\}} p_k(z_j) \right] p(\pi|Y_d(x), x) \\ &= p(Z|\emptyset, x)p(\emptyset|Y_d(x), x) \sum_{\pi \in \bar{\Pi}_{n,m}} \prod_{i: \pi(i) > 0} \frac{p_d(y_i, x)p_z(z_{\pi(i)}|y_i, x)}{(1 - p_d(y_i, x))\lambda p_k(z_{\pi(i)})} \end{aligned} \quad (9)$$

To gain intuition about the semantic observation model in this most general case, refer to Figure 3. With this model in hand, we can state the Bayesian filtering equations needed for semantic localization.

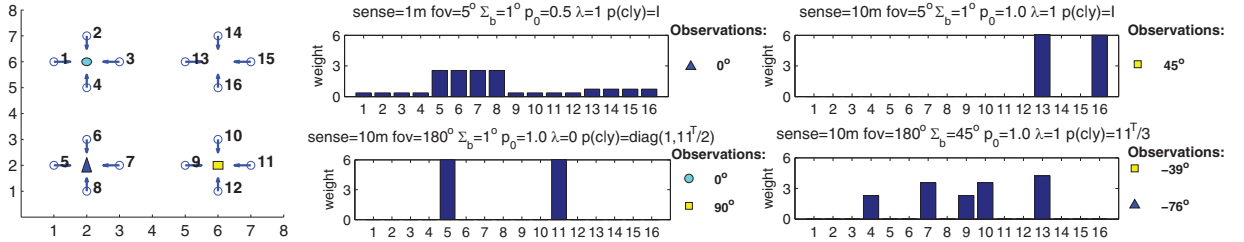


**Fig. 3.** Consider a localization scenario with 16 possible poses, indicated by the arrows on the left-most plot. There are three objects in the environment: a yellow square (class 1), a cyan circle (class 2), and a blue triangle (class 3). Initially, the 16 poses are equally likely (each has weight 1). Suppose that only a single set of semantic observations is received. The four plots to the right show how the likelihoods of the 16 locations change, depending on the received set. At each location, the likelihood of the semantic observation set is computed via (9) and normalized, so that the sum of the likelihoods is 16. The parameters, used in the semantic observation model, are listed at the top of the plots. For simplicity, the semantic observations here contain only bearing and class information.

---

**Algorithm 1.** Set-based particle filter.

---

- 1: **Input:** Particle set  $\{w_{t|t}^k, x_{t|t}^k\}_{k=1}^N$ , motion model pdf  $p_f$ , observation model pdf  $p$ , semantic map  $Y$ , control input  $u_t$ , set of semantic observations  $Z_{t+1}$
  - 2: **Output:** Particle set  $\{w_{t+1|t+1}^k, x_{t+1|t+1}^k\}_{k=1}^N$
  - 3: **for**  $k = 1, \dots, N$  **do**
  - 4:     **Predict:** Draw  $x_{t+1|t}^k$  from pdf  $p_f(\cdot | x_{t|t}^k, u_t)$
  - 5:      $w_{t+1|t}^k \leftarrow w_{t|t}^k$
  - 6:     **Update:**  $w_{t+1|t+1}^k \leftarrow p(Z_{t+1} | Y_d(x_{t+1|t}^k), x_{t+1|t}^k) w_{t+1|t}^k$
  - 7:      $x_{t+1|t+1}^k \leftarrow x_{t+1|t}^k$
  - 8: **Normalize the weights**  $\{w_{t+1|t+1}^k\}_{k=1}^N$  and re-sample if necessary
- 

**Proposition 1.** *The Bayesian recursion which solves the Semantic Localization problem is*

$$\begin{aligned} \text{Predict : } & p_{t+1|t}(x) = \int p_f(x|x', u_t) p_{t|t}(x') dx' \\ \text{Update : } & p_{t+1|t+1}(x) = \eta_{t+1} p(Z_{t+1} | Y_d(x), x) p_{t+1|t}(x) \end{aligned} \quad (10)$$

where  $p(Z_{t+1} | Y_d(x), x)$  is the random finite set observation model in (9) and  $\eta_{t+1}$  is a normalization constant.

#### 4. Approximating the set-based Bayes filter

While the Bayesian recursion with set-valued observations in Proposition 1 is theoretically appealing, like its vector-based counterpart, it is intractable. An accurate and efficient approximation to the set-based Bayes filter is, therefore, the subject of this section. The particle filter (Thrun et al., 2005: Ch.4) is an approximation to the Bayes filter with vector-valued observations, which has been very successful in practice for geometric localization. Since the robot state is still vector-valued, we represent its pdf  $p_{t|t}$  at time  $t$  with a set of particles  $\{w_{t|t}^k, x_{t|t}^k\}_{k=1}^N$ :

$$p_{t|t}(x) \approx \sum_{k=1}^N w_{t|t}^k \delta(x - x_{t|t}^k)$$

where  $\delta(\cdot)$  is a Dirac delta function. The particle-filter implementation of (10), with the motion model (1) as a proposal distribution, is summarized in Algorithm 1.

It appears standard with the exception that, instead of the conventional vector-based measurement update, line 6 requires computing the likelihood of the random set  $Z_{t+1}$  according to (9). As mentioned earlier, it is not apparent how to efficiently compute the sum over all data associations  $\pi$ . To gain intuition we begin with the simpler case of “perfect detection” in (5).

Fix a robot state  $x$  and consider the non-trivial case when the received measurements  $Z$  and the detectable landmarks  $Y_d(x)$  have the same cardinality  $m$ . We can think about the data association between  $Z$  and  $Y_d(x)$  from a graph-theoretic perspective. Represent the sets  $Y_d(x)$  and  $Z$  by the vertices of a complete balanced bipartite graph. In detail, let  $V_1 := Y_d(x)$  and  $V_2 := Z$  be the vertices and  $E$  be the complete set of edges. Associate the weight  $w_e := p_z(z|y, x)$  with every edge  $e := (z, y) \in E$  and consider the weighted bipartite graph  $G := (V_1, V_2, E, w)$ . The data associations  $\pi$ , between the objects  $V_1$  and the measurements  $V_2$ , in the “perfect detection” case (5), in fact, correspond to *perfect matchings* in  $G$ . Given a perfect matching  $\pi$ , the associated product term inside the sum in (5) corresponds to its weight. Then, the sum over all  $\pi$  corresponds to the sum of the weights of all perfect matchings in  $G$ , which

notably is equal to the permanent of the adjacency matrix of  $G$ .

**Definition 1** (Permanent). *The permanent of an  $n \times m$  matrix  $A = [A(i, j)]$  with  $n \leq m$  is defined as*

$$\text{per}(A) := \sum_{\pi} \prod_{i=1}^n A(i, \pi(i))$$

where the sum is over all one-to-one functions  $\pi : \{1, \dots, n\} \rightarrow \{1, \dots, m\}$ . If  $n > m$ , then  $\text{per}(A) := \text{per}(A^T)$ .

It is now clear that the likelihood of a set of semantic observations in the “perfect detection” case can be obtained by computing the permanent of a matrix.

**Proposition 2.** *The likelihood in (5) of a random finite set of semantic observations,  $Z = \{z_1, \dots, z_m\}$ , in the case of no false positives and no missed detections, with  $n := |Y_d(x)| = m$  detectable objects, satisfies*

$$p(Z|Y_d(x), x) = \frac{1}{n!} \text{per}(Q)$$

where  $Q$  is a  $n \times n$  matrix with  $Q(i, j) := p_z(z_j|y_i, x)$  and  $\{y_1, \dots, y_n\}$  is an enumeration of the set  $Y_d(x)$  of detectable objects.

The general case in (9), where both false positives and missed detections are possible can be analyzed using the same graph-matching intuition. The following is our main result and its proof appears in Appendix C.

**Theorem 1.** *Given a robot state  $x$  and set of detectable objects  $Y_d(x)$  with  $n := |Y_d(x)| > 0$ , the likelihood of a random finite set  $Z = \{z_1, \dots, z_m\}$  of semantic observations, with  $m > 0$ , when both false-positive and missed detections are possible satisfies:*

$$\begin{aligned} p(Z|Y_d(x), x) &= \frac{e^{-\lambda} \lambda^m}{m!} \prod_{z \in Z} p_\kappa(z) \prod_{y \in Y_d(x)} (1 - p_d(y, x)) \\ &\times \begin{cases} \frac{1}{m!} \text{per} \left( \begin{bmatrix} Q & I_n \\ 1_{m,m} & 1_{m,n} \end{bmatrix} \right), & n \leq m \\ \frac{1}{n!} \text{per} \left( \begin{bmatrix} Q^T & I_m \\ 1_{n,n} & 1_{n,m} \end{bmatrix} \right), & m \leq n \end{cases} \end{aligned} \quad (11)$$

where  $p_d(y, x)$  is the probability of detecting object  $y \in Y_d(x)$ ,  $\lambda$  is the expected number of false-positive detections with spatial pdf  $p_\kappa(\cdot)$ ,  $1_{n,m}$  is a  $n \times m$  matrix of all ones, and  $Q$  is a matrix with elements:

$$Q(i,j) := \frac{p_d(y_i, x)p_z(z_j|y_i, x)}{(1 - p_d(y_i, x))\lambda p_\kappa(z_j)}, \quad i = 1, \dots, n \\ j = 1, \dots, m$$

Theorem 1 maps the problem of determining the pdf of  $Z$  in the general case in (9) to the problem of finding the permanent of a  $(m+n) \times (m+n)$  square matrix. The problem is still computationally challenging because computing

the permanent of a matrix is #P-complete<sup>7</sup> (Valiant, 1979). However, Theorem 1 allows us to leverage the extensive literature on approximation algorithms for computing the matrix permanent. The proof of Theorem 1 reduces the problem of summing the weights of all matchings in an unbalanced bipartite graph to the problem of summing the weights of all perfect matchings in an unbalanced bipartite graph and then to the problem of summing the weights of all perfect matchings in a balanced bipartite graph. We could stop at the first reduction, which would require calculating the permanent of a rectangular matrix. The reason for the second reduction is that existing permanent-approximation algorithms are much better for square than for rectangular matrices.

An exact method for computing the permanent of a  $d \times d$  matrix, proposed by Ryser (1963) and later improved by Nijenhuis and Wilf (1978: Ch.23), is summarized in Algorithm 2. Its time complexity is  $\Theta(d2^{d-1})$ . The dimension of the matrix in (11) is equal to the number of detections returned by the vision algorithm plus the number of detectable objects within the sensor field of view, which in some cases is often small enough to enable a real-time implementation of Algorithm 2. Otherwise, there are a number of polynomial-time arbitrarily-close approximations to the permanent computation. For example, Jerrum et al. (2004) showed that for any  $\epsilon \in (0, 1]$  and  $\delta > 0$ , there exists a randomized algorithm whose output comes within a factor  $(1 \pm \epsilon)$  of  $\text{per}(A)$  with probability at least  $1 - \delta$  with a random running time  $T$  such that  $\mathbb{E}(T) = O(d^{10}(\log d)^3)$ . The running time was later improved by Bezáková et al. (2006) to  $O(d^7(\log d)^4)$ . Also, when  $A \in [0, 1]^{d \times d}$  is a matrix such that all row and column sums are at least  $\gamma d$  for  $\gamma \in (0.6, 1]$ , Law (2009: Ch.2.2) provides an algorithm with expected running time  $O(d^4(\log d + \epsilon^{-2} \log \delta^{-1}))$ .

**Proposition 3.** *Given  $m$  object detections and a semantic map with  $L$  objects, the time complexity of Algorithm 1 for semantic localization with  $N$  particles is  $O(N(m+L)2^{(m+L)})$ , if the measurement update is computed exactly with Algorithm 2, and  $O(N(m+L)^7(\log(m+L))^4)$  in expectation, if computed approximately via the randomized method of Bezáková et al. (2006).*

While the time complexity in Proposition 3 is in terms of  $L$ , the number of objects in the environment, the running time of the filter updates actually depends on  $n := |Y_d(x)|$ , the number of detectable objects within the field of view of each particle, which is typically much smaller than  $L$ . This, of course, critically depends on the assumption in (2) that the probability of detection is 0 outside of the sensor field of view. Thus, the dimension of the matrix, whose permanent needs to be calculated in (11), scales with the density of the detectable objects within the sensor field of view, rather than the environment size.

Using the idea of Theorem 1, similar results can be obtained for the simpler cases with no false positives or no

---

**Algorithm 2.** Permanent. Reproduced with kind permission from Elsevier (Nijenhuis and Wilf, 1978: Ch.23).

---

```

1: Input:  $d \times d$  matrix  $A$  Output:  $\text{per}(A)$ 
2: for  $i = 1, \dots, d$  do
3:    $x(i) \leftarrow A(i, d) - \frac{1}{2} \sum_{j=1}^d A(i, j)$ 
4:    $s \leftarrow -1, g \leftarrow \text{false}(d, 1), p \leftarrow s \prod_{i=1}^d x(i)$ 
5: for  $k = 2, \dots, 2^{d-1}$  do
6:   if  $k$  is even then  $j \leftarrow 1$                                 Obtain next gray code subset
7:   else  $\{j \leftarrow 2$ 
8:     while  $g_{j-1}$  is false do
9:        $j \leftarrow j + 1\}$ 
10:     $s \leftarrow -s, z \leftarrow 1 - 2g_j, g_j \leftarrow \text{not } g_j$ 
11:    for  $i = 1, \dots, d$  do
12:       $x(i) \leftarrow x(i) + zA(i, j)$ 
13:     $p \leftarrow p + s \prod_{i=1}^d x(i)$ 
14: return  $2(-1)^d p$ 

```

---

missed detections. Appendix D shows the link between the likelihood of a set of semantic observations and the matrix permanent for all cases.

## 5. Active semantic localization

The previous sections described the sensing model and the computational aspects of implementing a particle filter for localization using semantic observations. In this section, we emphasize that the observer can choose motion trajectories actively in order to improve the performance of the semantic localization. As before, let the pdf  $p_{t|t}$  of the pose at time  $t$  be represented by the particle set  $\{w_{t|t}^k, x_{t|t}^k\}_{k=1}^N$ . The main idea is to choose a sequence  $\sigma := u_t, \dots, u_{t+T-1}$  of control inputs for the next  $T$  time steps in order to minimize some measure of uncertainty in the pose. To simplify the notation going forward, assume, without loss of generality, that the current time is  $t = 0$ . We choose to use the entropy  $\mathbb{H}(x_{0:T}|Z_{1:T})$  of the current and future poses  $x_{0:T}$  conditioned on the future semantic observations  $Z_{1:T}$  as the uncertainty criterion. The conditional entropy is an appropriate objective because it quantifies the amount of information needed to describe the outcome of a random quantity (the future poses) given the value of another random quantity (the semantic observations) (Cover and Thomas, 2006). Conditional entropy and mutual information, a closely related measure of information, have been successfully applied to several active perception problems (Charrow et al., 2013; Karasev et al., 2012). Here, we consider the following problem.

**Problem 2** (active semantic localization). *Given a prior pdf of the pose  $x_0$ , the semantic map  $Y$ , and a space  $\Sigma := \{\sigma^i | \sigma^i := u_0^i, \dots, u_{T-1}^i\}_{i=1}^M$  of possible control sequences of length  $T$ , choose the sequence  $\sigma^*$ , which minimizes the entropy of the current and future poses  $x_{0:T}$  conditioned on the future semantic observations  $Z_{1:T}$ .*

$$\begin{aligned} \sigma^* \in \arg \min_{\sigma \in \Sigma} & \mathbb{H}(x_{0:T}|Z_{1:T}) \\ \text{subject to} & x_{s+1} \sim p_f(\cdot|x_s, \sigma_s), \quad s = 0, \dots, T-1 \\ & Z_s \sim p(\cdot|Y_d(x_s), x_s), \quad s = 1, \dots, T \end{aligned} \quad (12)$$

where  $p_f$  is the motion model (1) and  $p(\cdot|Y_d(x), x)$  is the semantic observation model (11).

Note that the active semantic localization problem as stated in (12) is much simpler than a problem which asks for a closed-loop control policy, minimizing the conditional entropy. Reinforcement learning or dynamic programming approaches can be used to learn such a control policy but the complexity would be much worse than that of the solution we offer here. In (12), the number of states, at which the cost function needs to be evaluated, scales linearly with the number of motion primitives in  $\Sigma$  and the number of particles in the prior pose distribution since only the reachable set of pose pdfs need to be considered. In contrast, an approach for computing a control policy would need to consider the space of all possible pdfs and evaluate the cost function over it. As we show below, evaluating the cost function in (12) even a single time is computationally very challenging.

An important research question, which we do not address here, is: “How should the set  $\Sigma$  of control sequence in (12) be chosen?”. Instead, we focus on evaluating the entropy criterion in (12) for a given sequence  $\sigma \in \Sigma$  efficiently. We assume that  $\Sigma$  has been designed offline and consists of motion primitives, each with  $T$  sampling poses, that can provide reasonable coverage of the robot’s surroundings. Sixty locations with outward facing orientations were chosen on the perimeter of a circle of radius 10 m. A differential-drive controller was used to generate a control sequence of length  $T = 5$ , which would lead a robot at the origin to each of the selected locations. Figure 4 shows the resulting set of motion primitives. They are wavy because the controller tries to follow a straight using a discrete set

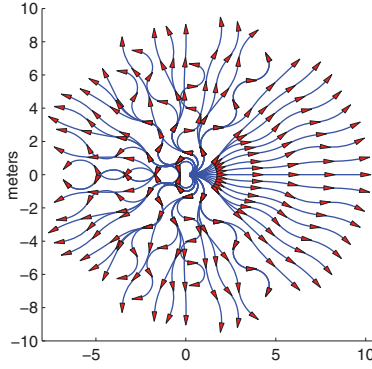


**Fig. 4.** The set of motion primitives used for active localization. Each segment contains five measurement poses indicated by the red triangles.

of velocity and angular-velocity input. The waviness provides measurement points with different orientations which is advantageous for localization because the measurements, collected along the way, would be diverse.

### 5.1. Minimizing conditional entropy

While accuracy is of utmost importance for the inference (filtering) process, speed is crucial for the planning process in (12). At each time step, the inference process needs to be carried out for a single set of observations (the actual one), but the planning process needs to envision various measurement realizations and various robot responses. Since it is desirable to plan with many control sequences and for long time horizons, in essence, the inference process needs to be carried out many times at each planning step. If there is to be any hope for real-time planning, computing the objective function in (12) needs to be extremely efficient.

Given a control sequence  $u_{0:T-1}$ , the conditional entropy is defined as follows:

$$\begin{aligned} \mathbb{H}(x_{0:T}|Z_{1:T}) := & \int \left[ \int -g(x_{0:T}, Z_{1:T}, u_{0:T-1}) \log g(x_{0:T}, Z_{1:T}, u_{0:T-1}) dx_{0:T} \right] \\ & p(Z_{1:T}) dZ_{1:T} \end{aligned} \quad (13)$$

where  $p(Z_{1:T})$  is the (not conditional) pdf of the semantic observations and we have defined

$$\begin{aligned} g(x_{0:T}, Z_{1:T}, u_{0:T-1}) := & \\ & \frac{p_{0|0}(x_0) \prod_{s=1}^T p_f(x_s|x_{s-1}, u_{s-1}) \prod_{s=1}^T p(Z_s|Y_d(x_s), x_s)}{p(Z_{1:T})} \end{aligned} \quad (14)$$

using the assumption that the sets  $Z_{1:T}$  are conditionally independent, given the set of detectable objects  $\bigcup_{s=1}^T Y_d(x_s)$  and the trajectory  $x_{1:T}$ . This definition makes efficient computation seem hopeless. Even if the

measurement sets  $Z_{1:T}$  were given, the inside integral in (13) would need to be evaluated for each of the  $M$  control sequences with  $N^{T+1}$  future particle evolutions, each requiring  $T$  evaluations (permanent computations) of the semantic observation likelihood. Assuming exact permanent computations, this makes the complexity of obtaining just the inside integral:  $O(MN^{T+1} \sum_{s=1}^T (|Y| + |Z_s|) 2^{|Y| + |Z_s|})$ ! In order to address the complexity of this planning problem we will use several approximations.

*Maximum likelihood data association* First, during the planning process, there is no hope for data association via the permanent. We resort to maximum likelihood data association. Given a set  $Z$  of semantic observations with  $m := |Z|$ , for each particle  $x$ , we construct an association function  $\pi : \{1, \dots, m\} \rightarrow \{0, 1, \dots, |Y_d(x)|\}$  by processing the measurements  $z_j, j = 1, \dots, m$  sequentially. For  $z_j$ , we compute

$$\max \left\{ \max_{i \in \{1, \dots, |Y_d(x)|\}} p_d(y_i, x) p_z(z_j|y_i, x), \frac{\lambda}{|Z| - q} p_\kappa(z_j) \right\}$$

where  $q$  is the number of measurements already assigned to clutter, and let  $\pi(j) = i$ , if the max is achieved at a detectable object  $y_i \in Y_d(x)$ , and  $\pi(j) = 0$ , otherwise. Then, the likelihood of  $Z$  is

$$\begin{aligned} p(Z|Y_d(x), x, \pi) = & \frac{e^{-\lambda}}{|Z|!} \prod_{j|\pi(j)=0} \lambda p_\kappa(z_j) \prod_{y \in D} (1 - p_d(y, x)) \\ & \prod_{j|\pi(j)>0} p_d(y_{\pi(j)}, x) p_z(z_j|y_{\pi(j)}, x) \end{aligned}$$

where  $D$  is the set of unassigned detectable objects. The use of maximum likelihood data association in (14) replaces the  $O\left(\sum_{s=1}^T (|Y| + |Z_s|) 2^{|Y| + |Z_s|}\right)$  cost of permanent computations by  $O\left(\sum_{s=1}^T |Z_s| |Y|\right)$ .

*Noiseless motion* Another problematic term in the computational-complexity characterization of the inner integral in (13) is  $N^{T+1}$ . It is due to the evolution of the set of  $N$  particles over the planning horizon  $T$ . The integral can be simplified significantly by neglecting the noise in the motion model (1). In other words, the robot can be optimistic and plan its future trajectories with a “perfect motion” assumption (albeit not satisfied in reality):

$$p_f(x_{s+1}|x_s, u_s) = \delta(x_{s+1} - f(x_s, u_s, 0)) \quad (15)$$

For the given control sequence  $u_{0:T-1}$ , let the (now) deterministic evolution of the particles in the initial particle set  $\{w_{0|0}^k, x_{0|0}^k\}$  over the time horizon  $s = 0, \dots, T-1$  be  $x_{s+1|s+1}^k := f(x_{s|s}^k, u_s, 0)$ . Then, the “perfect motion” assumption implies that

$$\begin{aligned} g(x_{0:T}, Z_{1:T}, u_{0:T-1}) & \\ & = \sum_{k=1}^N \frac{w_{0|0}^k \prod_{s=1}^T p(Z_s|Y_d(x_{s|s}^k), x_{s|s}^k)}{p(Z_{1:T})} \prod_{s=0}^T \delta(x_{s|s}^k - x_s) \end{aligned}$$

which in turn reduces the integral in (13) to

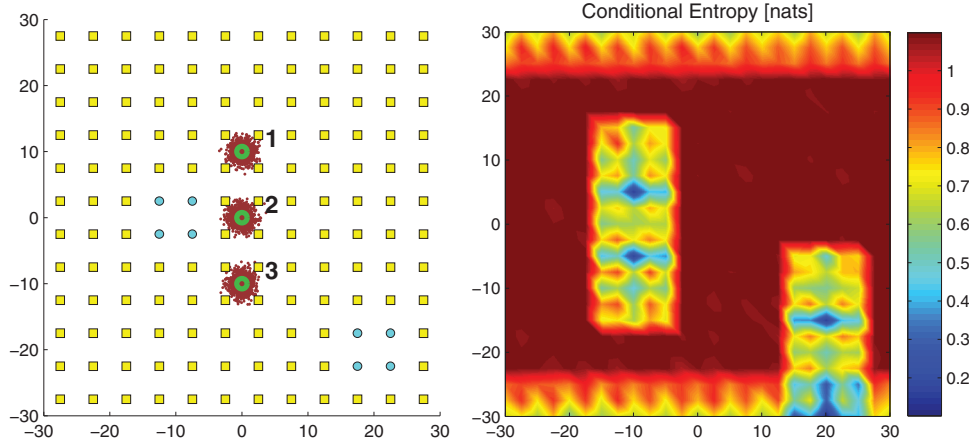


**Fig. 5.** The left plot shows a simulation of a 2-D localization scenario with two object classes (circle, square). The prior density of the observer’s pose is represented by the dark red particle set, which is concentrated in three locations (green). The observer has a field of view of  $360^\circ$  and a sensing range of 4 m. The other parameters of the observation model were  $p_0 = 0.73$ ,  $m_0 = 2.7$ ,  $v_0 = 35$ ,  $\Sigma_\beta = 4^\circ$  and  $\lambda = 0.5$ . The right plot shows the entropy of the observer’s location (in the local frame of reference) conditioned on one set of semantic observations. As the summarized particle set contains only three particles, the entropy varies from 0 to 1.099 nats.

$$H(x_{0:T}|Z_{1:T}) = \int \left[ -\sum_{k=1}^N \tilde{w}^k(Z_{1:T}) \log \tilde{w}^k(Z_{1:T}) \right] p(Z_{1:T}) dZ_{1:T} \quad (16)$$

where

$$\tilde{w}^k(Z_{1:T}) := \frac{w_{0|0}^k \prod_{s=1}^T p(Z_s|Y_d(x_{s|s}^k), x_{s|s}^k)}{p(Z_{1:T})} \quad (17)$$

are the normalized weights of the (updated) particle set at time  $T$ . Note that, above,  $p(Z_{1:T})$  is a normalization factor and does not need to be computed explicitly. Combining the result in (16) with maximum likelihood data association, reduces the computational complexity of the inner integral (now a sum) in (13) from  $O(MN^{T+1} \sum_{s=1}^T (|Y| + |Z_s|) 2^{|Y|+|Z_s|})$  to  $O(MN|Y| \sum_{s=1}^T |Z_s|)$ . Most importantly, the new complexity does not have an exponential dependence on the problem parameters.

*Particle set summarization* A final reduction in complexity can be obtained by decreasing the number of particles that represent the prior pose distribution. Intuitively, for planning purposes, it is not crucial to represent the distribution accurately but rather to ensure that it contains the competing hypotheses. Charrow et al. (2013) proposed replacing subsets of similar particles with their average in the context of target tracking with range-only sensing. The authors prove that for Gaussian measurement noise, the approximation introduces a bounded error in the mutual information between the observations and the target state. We adopt the same idea here, despite that the measurement noise (except the bearing noise) is not Gaussian. Specifically, we partition the robot state space with a regular square grid and replace the particles, contained in the

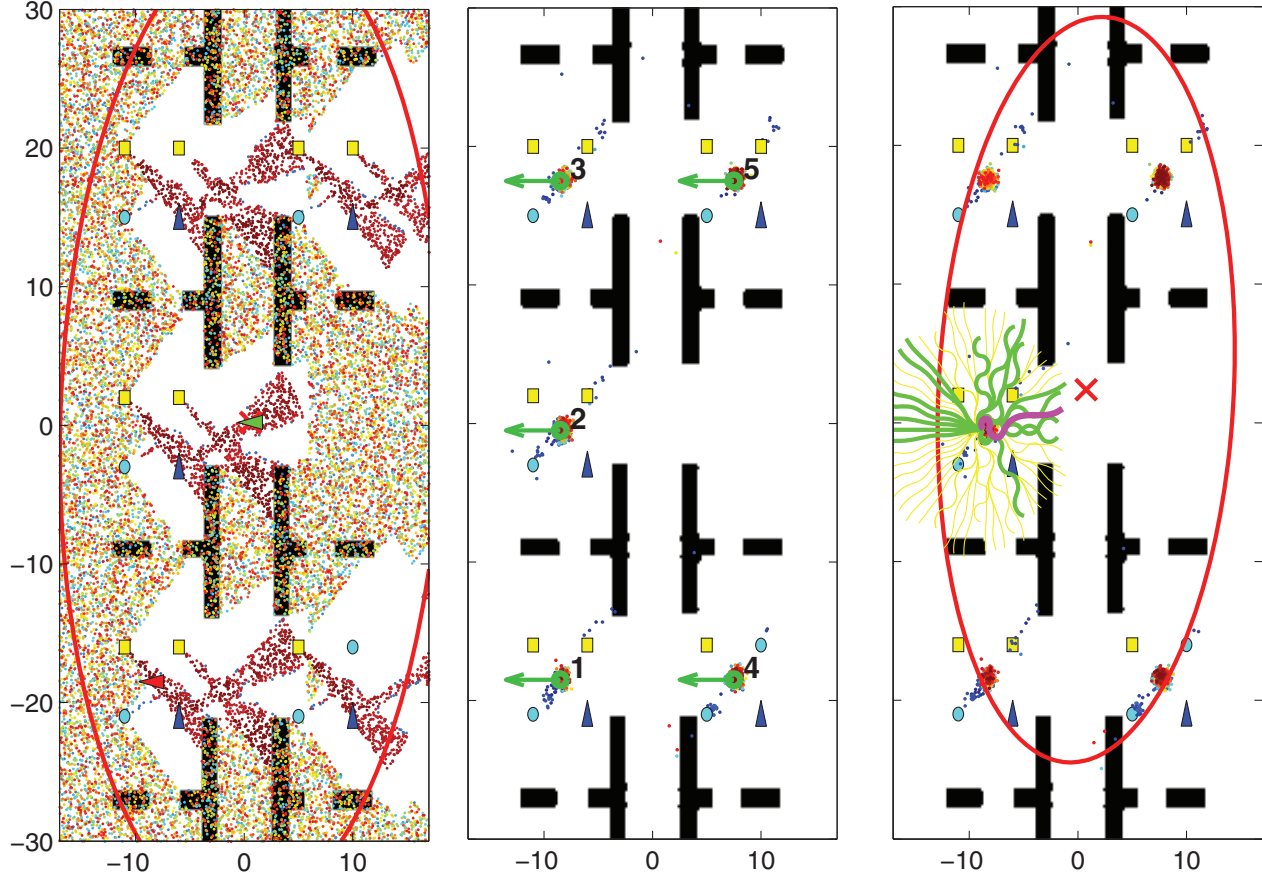
same cell, with their weighted average. Depending on the size of grid cells, this approximation can reduce the number of particles significantly (see Figure 5). We emphasize that all of these approximations (particle summarization, noiseless motion, maximum likelihood data association) are used only in the planning process. The inference process still uses the full particle set, the full semantic observation model in (11), and considers motion noise.

Now, that the evaluation of the inner integral in (13) has been simplified significantly, we consider the outside integration over the set-valued variables  $Z_{1:T}$ . Since not even the cardinality of the measurement sets is known, an exact computation would be hopeless. However, given a robot trajectory, the semantic map  $Y$  and the semantic observation model (11) can be used to simulate measurements from the detectable objects and, in turn, obtain a Monte Carlo approximation to (13).

*Monte Carlo integration* The key, to a fast and accurate Monte Carlo approximation of (13), is to simulate measurement sets from  $p(Z_{1:T})$  in a way that the samples are concentrated in regions that make large contributions to the integral. Observe that, due to the particle set approximation of the prior  $p_{0|0}$  and the “perfect motion” assumption,  $p(Z_{1:T})$  is a finite mixture model:

$$\begin{aligned} p(Z_{1:T}) &= \int p(Z_{1:T}, x_{0:T}) dx_{0:T} \\ &= \int \prod_{s=1}^T p(Z_s|Y_d(x_{s|s}^k), x_{s|s}^k) \delta(x_{s|s}^k - x_s) p_{0|0}(x_0) dx_{0:T} \\ &= \sum_{k=1}^N w_{0|0}^k \prod_{s=1}^T p(Z_s|Y_d(x_{s|s}^k), x_{s|s}^k) \end{aligned}$$

An efficient way to sample from the mixture model  $p(Z_{1:T})$  is to first sample the mixture component according



(A) Particle set after the first set of semantic observations, particle mean (green triangle), particle covariance (red ellipse), and the actual unknown robot pose (red triangle)

(B) The particle distribution converges to 5 ambiguous poses (green arrows) after several semantic observations. Pose 4, unlike the rest, has two cyan circles in its vicinity.

(C) All motion primitives (yellow, in frame of reference of pose 2), minimum-collision-probability motion primitives (green), and minimum-entropy-and-collision-probability motion primitive (magenta)

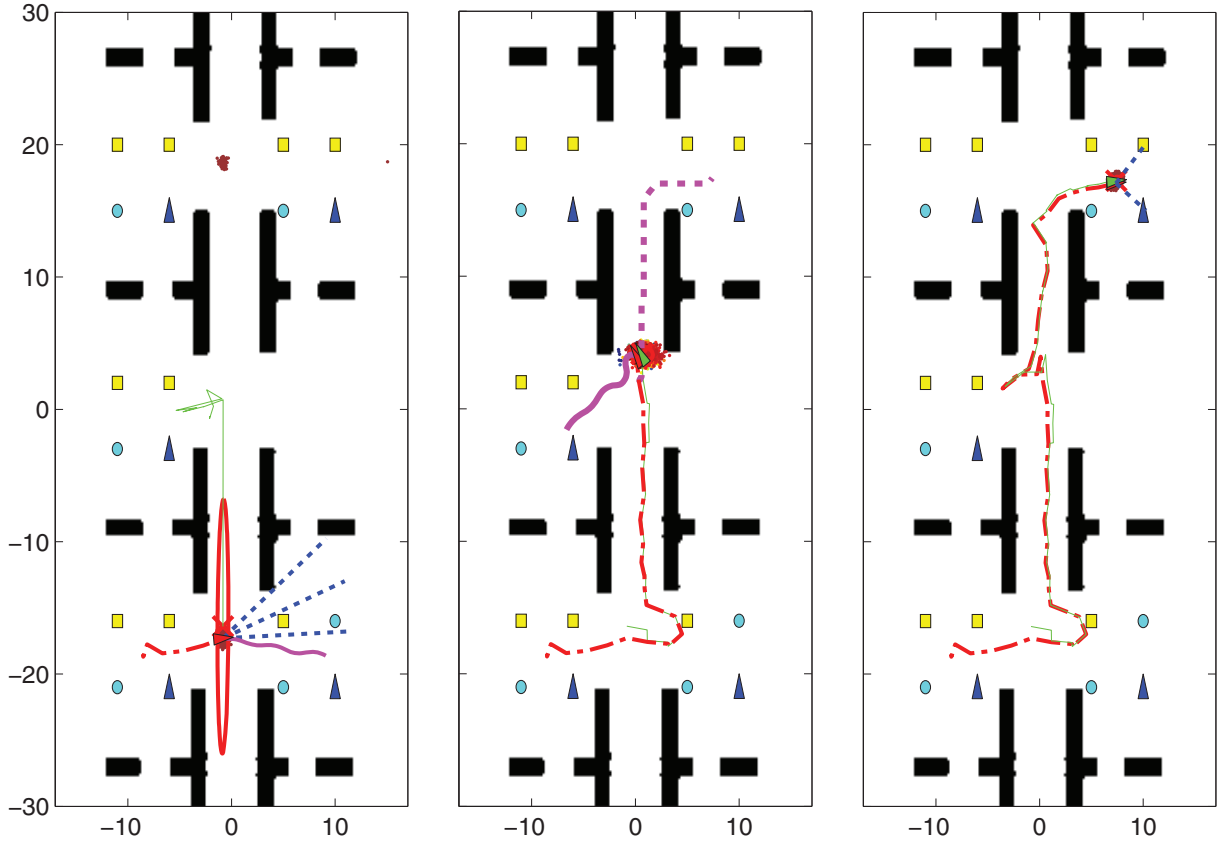
**Fig. 6.** A simulation of a differential-drive robot employing our active semantic localization approach to reach a goal. The environment contains objects from three classes (square, circle, and triangle) in six areas, divided by the black obstacles. The task of the robot is to localize itself (position and orientation) and reach pose 5, indicated by the green arrow on subplot (b). It has a field of view of  $94^\circ$  and a sensing range of 12.5 m. The other parameters of the observation model were  $p_0 = 0.73$ ,  $m_0 = 2.7$ ,  $v_0 = 35$ ,  $\Sigma_\beta = 5^\circ$ , and  $\lambda = 0.5$ . The robot had no prior information about its initial pose (A). The particle distribution converges to 5 ambiguous locations after several semantic observations because a yellow square and a cyan circle are detected repeatedly (B). The robot plans its motion (using the motion primitives in Figure 4) to minimize the probability of collision and the entropy of its pose, conditioned on five future sets of semantic observations (C). The description continues in Figure 7.

to the weight  $w^k$  and then sample each  $Z_s$  from the conditional densities. This has the additional benefit of sampling observation sets that are likely to be encountered by the robot and should provide a large contribution to the integral. Thus, for a given control sequence  $u_{0:T-1}$ , we follow the following steps to estimate  $\mathbb{H}(x_{0:T}|Z_{1:T})$ :

1. sample a particle  $x_{0|0}^l$  from the prior particle set according to the weights  $w_{0|0}^k$ ,  $k = 1, \dots, N$ ;
2. compute the particle trajectory  $x_{s+1|s+1}^l := f(x_{s|s}^l, u_s, 0)$  for  $s = 0, \dots, T - 1$ ;

3. sample  $Z_s^l$  from the semantic observation model  $p(Z_s^l|Y_d(x_{s|s}^l), x_{s|s}^l)$  for  $s = 1, \dots, T$ ;
4. compute the normalized updated particle weights  $\tilde{w}^k(Z_{1:T}^l)$  via (17) for  $k = 1, \dots, N$ ;
5. evaluate the inner sum:  $H_l := -\sum_{k=1}^N \tilde{w}^k(Z_{1:T}^l) \log \tilde{w}^k(Z_{1:T}^l)$ ;
6. repeat the above steps  $N_z$  times to obtain the Monte Carlo approximation,  $\mathbb{H}(x_{0:T}|Z_{1:T}) \approx \frac{1}{N_z} \sum_{l=1}^{N_z} H_l$ .

Figure 5 shows a Monte Carlo approximation of the entropy of the robot pose, conditioned on a single future observation set, in a simulated 2-D environment. The



(A) Actual robot trajectory (dotted red), estimated trajectory (green), particle distribution (dark red), particle covariance (red ellipse), and observation set (dotted blue lines) after the second cyan circle in area 4 (bottom right) is observed

(B) Actual (dotted red) and estimated (green) robot trajectories, intended trajectory towards the goal (dotted magenta), and minimum-entropy-and-collision-probability motion primitive (solid magenta) chosen to decrease the pose uncertainty

(C) The robot managed to re-localize itself and reach the goal successfully

**Fig. 7.** Continuation of the active semantic localization simulation from Figure 6. The robot recognizes correctly that the best way to disambiguate its pose is to visit the bottom-right area (A). At this point, there are only two remaining hypotheses and more weight is starting to concentrate around the true pose. Once the robot considers itself localized (the covariance of the particle set is small), it plans a path to the goal in the top-right area. As there are no landmarks along the hallway, the motion noise causes the uncertainty in the robot pose to increase. Using the entropy-minimization criterion, the robot recognizes that it needs to deviate from its intended path and visit an area with landmarks in order to re-localize (B). The robot reaches the goal successfully (C).

results hint at several important considerations regarding active localization. In particular, there is a correlation, among the landmark distribution in the environment, the sensing range and field of view of the robot, and the length of the planning horizon  $T$ , which affects the performance. On the one hand, if the sensing range and the field of view are unrestricted, there would be no need to for active localization. The filtering process alone will be able to uniquely identify the robot pose. On the other hand, since the planning process is inherently local, if the horizon  $T$  is not long enough to reach perceptually distinct areas in the environment, the robot can get stuck in a local maximum (the flat red region in Figure 5) of the entropy surface. Then, all considered motions will have the same cost and no progress will be made. Active localization becomes particularly

attractive when the sensing range and the field of view are limited but the environment contains distinct landmarks within the reachable (in  $T$  steps) sensing perimeter. In such scenarios, the planning process can improve both the efficiency and accuracy of the localization filter.

## 5.2. Localization as a secondary objective

Often times, localization is a requisite but secondary objective for a mobile robot. In addition, a robot typically needs to avoid collisions and reach a primary objective, such as a goal pose in the environment. In this section, we discuss how to combine the active semantic localization with collision avoidance and path-planning to a goal pose. First, as discussed by Fox et al. (1998), an additional term can be

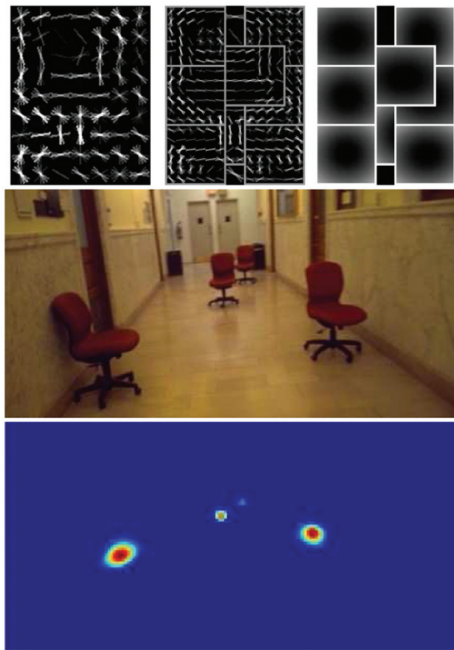


**Fig. 8.** A component of the deformable part model of a chair (top) and scores (bottom) from its evaluation on an image (middle) containing four chairs.

added to the cost function in order to minimize the probability that a control sequence leads to a collision. Dealing with obstacles in the environment correctly also requires that object visibility is accounted for both in the probability of detection  $p_d(y, x)$  and in the sampling of measurement sets for the Monte Carlo evaluation of the conditional entropy. Second, once the robot is localized well, it can plan a global path  $\mathcal{P} = \{\rho\}$ , consisting of a sequence of poses  $\rho$ , which leads the robot to its ultimate goal. Along the way, if re-localization is necessary the robot should not deviate significantly from the intended path  $\mathcal{P}$ . Thus, we consider the following three-fold objective:

$$\begin{aligned} \sigma^* \in \operatorname{argmin}_{\sigma \in \Sigma} \quad & \alpha_1 \mathbb{H}(x_{0:T} | Z_{1:T}) + \alpha_2 \mathbb{E} \left[ \min_{\rho \in \mathcal{P}} d(x_T, \rho) \right] \\ & + \alpha_3 \max_{s=1}^T \mathbb{P}(x_s \in \text{Collision}) \\ \text{subject to} \quad & x_{s+1} \sim p_f(\cdot | x_s, \sigma_s), s = 0, \dots, T-1 \\ & Z_s \sim p(\cdot | Y_d(x_s), x_s), s = 1, \dots, T \end{aligned}$$

where  $\mathbb{E}[\min_{\rho \in \mathcal{P}} d(x_T, \rho)]$  is the expected minimum deviation of the final motion sequence pose  $X_T$  from the global path  $\mathcal{P}$  and  $\max_{s=1}^T \mathbb{P}(x_s \in \text{Collision})$  is the maximum probability of collision along the chosen trajectory. The constants  $\alpha_1, \alpha_2, \alpha_3$  specify the relative importance of the three objectives. Due to the “perfect motion” assumption, the last two terms in the cost function can be computed as follows:

$$\begin{aligned} \max_{s=1}^T \mathbb{P}(x_s \in \text{Collision}) &= \max_{s=1}^T \left( \sum_{k=1}^N 1\{x_{s|s}^k \in \text{Collision}\} w_{0|0}^k \right) \\ \mathbb{E} \left[ \min_{\rho \in \mathcal{P}} d(x_T, \rho) \right] &= \sum_{k=1}^N \left( \min_{\rho \in \mathcal{P}} d(x_{T|T}^k, \rho) \right) w_{0|0}^k \end{aligned} \quad (18)$$

where  $1\{x_{s|s}^k \in \text{Collision}\}$  is the indicator of the set  $\{x_{s|s}^k \in \text{Collision}\}$ .

The performance of the active semantic localization approach is demonstrated in simulation with a differential-drive robot in Figure 6 and Figure 7. The task of the robot is to localize itself globally and autonomously and subsequently reach a goal pose specified on the prior map. The initial particle set is uniformly distributed over the whole environment. In the early iterations, minimizing the entropy will be expensive and of little value. In our experiments, the robot either acquires several observation sets without moving (as in Figure 6(A)) or chooses motion primitives which minimize the collision probability only (by setting  $\alpha_1 = 0, \alpha_2 = 0, \alpha_3 = 1$ ). Once the summarized particle set contains less hypotheses, both the entropy and the probability-of-collision criteria can be enabled to select informative trajectories (see Figure 6(B) for details). We used  $\alpha_1 = 0.55, \alpha_2 = 0, \alpha_3 = 0.45$  before the first time the robot is localized well (the covariance of the particle set is small). Once well-localized, the robot can plan a path from the mode of the distribution to the goal pose. In our experiments, we used  $A^*$  with a cost map that rewards landmark visibility. If along the way to the goal the uncertainty in the robot pose starts to increase due to the motion noise, the robot can carry out the minimization in (18) with all three terms enabled. We used  $\alpha_1 = 0.5, \alpha_2 = 0.05, \alpha_3 = 0.45$  in this case (see Figure 7(B) for details). The experiments demonstrate that the robot achieves global localization autonomously, avoids collisions in the environment, re-localizes itself if necessary, and reaches the goal pose successfully. Additional simulations, which compare our approach to other active localization techniques, are presented in Section 6.4.

## 6. Performance evaluation

This section evaluates the performance of our approach in simulation and in two real-world scenarios. Global localization from semantic observations is demonstrated for a differential-drive robot in Section 6.1 and for a Tango phone (Google ATAP group, 2014) in Section 6.2.

Semantic information was obtained using deformable part models (DPM; Felzenszwalb et al., 2010), which achieve state-of-the-art performance in single-image object recognition. Given an input image, an image pyramid is obtained via repeated smoothing and subsampling. Histograms of oriented gradients are computed on a dense grid at each level of the pyramid. For each object class (in the set  $\mathcal{C}$ ), a detector is applied in a sliding-window fashion to the image pyramid, in order to obtain detection scores at each pixel and scale (see Figure 8). The detection scores above a certain threshold are returned, along with bounding box, class, and bearing information. The collection of all such measurements at time  $t$  forms the random finite set  $Z_t$ . A significant increase in detection speed is obtained via the active approach of Zhu et al. (2014), which optimizes the order of filter evaluations and the time at which to stop and make a decision.

In our experiments, it was sufficient to represent the state of an object  $y$  with its position and class because orientation and appearance variations are captured well by a DPM-based detector. If necessary, our model can incorporate rich appearance and shape signatures by extending the object state  $y$  and training an appropriate observation model. This is likely to make the data association more unimodal (i.e. make the terms in the sum in (9) dominated by the weight of a single data association), in which case the maximum likelihood data association approach (Section 5.1.1) would perform well. We emphasize that the permanent approach can handle this scenario efficiently too. As permanent approximation methods rely on Monte-Carlo sampling from the data associations, fewer samples can be used to speed up the computations. The connection between the observation model and the permanent incorporates this naturally and leverages state-of-the-art algorithms.

### 6.1. Mobile robot semantic localization

*Robot platform.* We carried out simulations and real-world experiments in an indoor environment using a differential-drive robot equipped with an inertial measurement unit (IMU), magnetic wheel encoders, a Kinect RGB-D camera with Nyko Zoom wide-angle lens, and a Hokuyo UTM-30LX 2D laser range finder. The IMU and the encoders were integrated using a differential-drive model and Gaussian noise was added to obtain the motion model in (1). Only the RGB images were used for semantic observations. The depth was not used, while the lidar was used to provide a ground-truth trajectory in the real-world experiments, via geometric Monte Carlo localization. Algorithm 1 was used for semantic localization. The measurement updates were performed using the exact permanent algorithm (Algorithm 2). The performance is demonstrated for *global localization*, which means that the robot had no prior information about its initial pose.

The detection model  $p_d(y, x)$ , the measurement likelihood  $p_z(z|y, x)$ , and the clutter model  $p_\kappa(z)$  were obtained from training data as discussed in Section 3.1. The angle of view of the wide-angle lens was  $94^\circ$ , the detection range 10 m, and the following parameters were learned:  $p_0 = 0.92$ ,  $m_0 = 3.5$ ,  $v_0 = 20.52$ , and  $\Sigma_\beta = 4^\circ$ . The semantic map in the real-world experiment contained doors (class 1) and chairs (class 2). The confusion matrix was

$$p_c(c|y^c) = \begin{bmatrix} 0.94 & 0.08 \\ 0.06 & 0.92 \end{bmatrix}$$

while the detection score likelihood is shown in Figure 16.

*Simulation results.* A simulated environment of size  $25 \times 25 \text{ m}^2$  was populated by objects with randomly-chosen positions and classes (see Figure 12). The robot motion was simulated along a pre-specified trajectory. Semantic observations were simulated using the learned detection, clutter, and measurement likelihood models. The error in the estimates, averaged over 50 repetitions with

different randomly-generated scenes, is presented in Figure 15. Since the robot starts with a uniform prior over the whole environment, the error is large in the initial iterations. Multiple hypotheses are present until enough semantic measurements are obtained to localize the robot uniquely. The performance is also demonstrated in a challenging scenario with a lot of ambiguity in Figure 13. The reason for using only two classes in the experiments was to increase the ambiguity in the data association. Our approach can certainly handle more classes and a higher object density. Figure 14 shows a simulation with clutter rate  $\lambda = 4$  and 150 objects from 5 classes in a  $25 \times 25 \text{ m}^2$  area. Scenarios with such high object density necessitate the use of an approximate permanent algorithm for real-time operation.

*Real experiments.* The robot was driven through a long hallway containing doors and chairs. Four data sets were collected from the IMU (at 100 Hz), the encoders (at 40 Hz), the lidar (at 40 Hz), and the RGB camera (at 1 Hz). Lidar-based geometric localization was performed via the ROS amcl package (Howard and Gerkey, 2002) and the results were used as the ground truth. Extension 1 contains a video of the experiment. The lidar and semantic estimates of the robot trajectory are shown in Figure 9. The error between the two, averaged over the four runs, is presented in Figure 17. The error is large initially because, unlike the lidar-based localization, our method was started with an uninformative prior. Nevertheless, after the initial global localization stage, our approach achieves average errors in the position and orientation estimates of less than 35 cm and  $10^\circ$ , respectively. The particle filter evolution is illustrated in Figure 11 along with some object detections.

*Comparison with maximum likelihood data association.* We compared our permanent-based data association (PER) approach to the more traditional maximum likelihood data association (MLD) approach, used for example in FastSLAM (Montemerlo and Thrun, 2003). PER is based on Algorithm 1 with an exact permanent computation (Algorithm 2) on line 6. MLD is based on Algorithm 1 also but the set of detections on line 6 is processed sequentially as described in Section 5.1.1. The two approaches were compared on the four real datasets (Figure 9) and on the simulations in Figures 12 and 13. Because we assume semantically-meaningful measurements, the observation sets in our comparison had relatively low cardinalities. Of course, if there are many observations per time step (e.g. SIFT features), MLD would be significantly more efficient than the exact permanent algorithm. In future work, we plan to compare MLD with our approach with an approximate permanent computation.

The performance is presented in Table 1 for two types of initializations: local (L), for which the initial particle set had errors of up to 1 m and  $30^\circ$ , and global (G), for which the set was distributed uniformly over the environment. MLD(L) performs as well as PER(L) in the real experiments and in Figure 13. In Figure 12, the data association

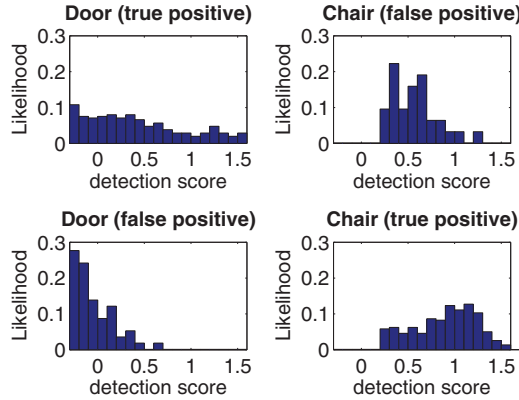


**Fig. 9.** Robot trajectories estimated by lidar-based geometric localization (red), image-based semantic localization (blue), and odometry (green) in the real experiment described in Section 6.1. The starting position, the door locations, and the chair locations are denoted by the red cross, the yellow squares, and the cyan circles, respectively. See Extension 1 for more details.

is highly multi-modal and MLD(L) does not converge even with 15,000 particles. This is reinforced in the global initialization cases. While PER(G) performs well with 3000 particles, MLD(G) needs 40,000 to converge consistently on the real datasets and is slower at the same level of robustness. In Figure 12 and Figure 13, MLD(G) does not converge even with 100,000 particles. We conclude that once the particles have converged correctly MLD performs as well as PER. However, with global initialization or ambiguous data association, MLD makes mistakes and can never recover, while PER is robust with a small number of particles.

## 6.2. Global localization for Project Tango

The Project Tango phone (Google ATAP group, 2014) is designed to track its full 3-D motion and create a geometric map of the environment. However, it does not use an absolute reference to the world and provides localization, only with respect to its initial frame of reference. We demonstrate that our semantic localization approach can provide global positioning of the Tango phone within an existing map of semantically meaningful landmarks.

The Tango phone is equipped with an IMU, a front-facing ( $120^\circ$  field of view) camera, a rear-facing RGB/IR narrow ( $68^\circ$  field of view) camera, and a rear-facing fish-eye ( $180^\circ$  field of view) camera. It provides a 6-D position-quaternion estimate of its pose and associated covariance, over time, within the initial frame of reference. In our experiments, this local trajectory was used as the motion model (1) in the prediction step in Algorithm 1. The update step was performed using semantic observations (class, score, and bearing) only from the narrow camera RGB images. The same hallway, as in the robot experiment (Section 6.1), was traversed several times with the phone. RGB images from the narrow camera (at 30 Hz) and the Tango visual odometry (at 30 Hz) were recorded. The prior semantic map of the environment (see Figure 10) contained doors (class 1), red chairs (class 2), and brown chairs (class 3). Two of the runs were used to train the object detector and to learn the observation model parameters: sensing range  $15\text{ m}$ ,  $p_0 = (0.71 \quad 0.81 \quad 0.82)^T$ ,  $v_0 = 35.4$ ,  $m_0 = 2.7$ ,  $\Sigma_\beta = 5^\circ$ ,  $\lambda = 0.76$ , and confusion matrix:

$$p_c(c|y^c) = \begin{bmatrix} 0.98 & 0 & 0 \\ 0 & 0.94 & 0.08 \\ 0.02 & 0.06 & 0.92 \end{bmatrix}$$

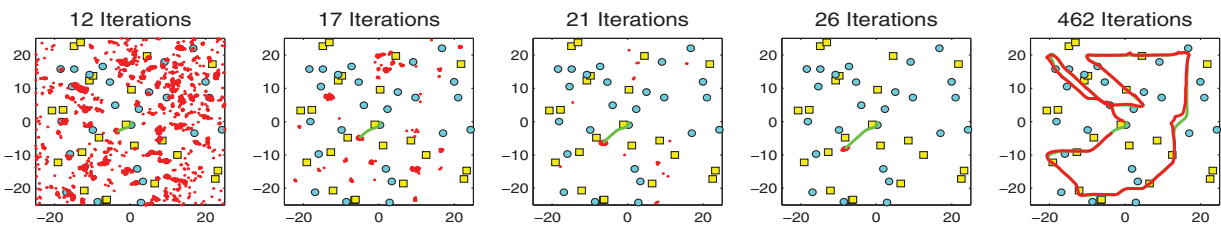


**Fig. 10.** Tango phone trajectory (red) estimated via semantic localization in the real experiment described in Section 6.2. The semantic map contains doors (yellow squares), red chairs (cyan circles), and brown chairs (blue triangles). Ground-truth information is not available for this experiment. See Extension 3 for more details.

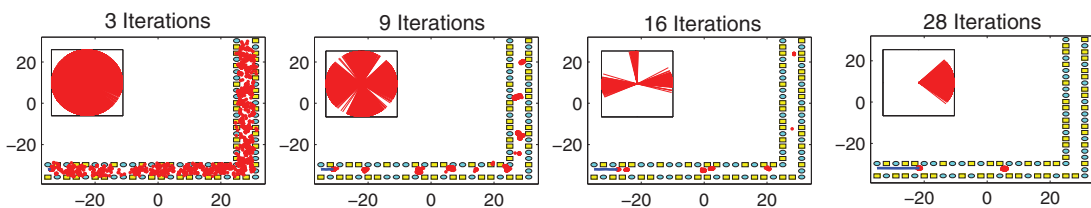


**Fig. 11.** Particle filter evolution (bottom) and object detections (top) during a real semantic localization experiment.

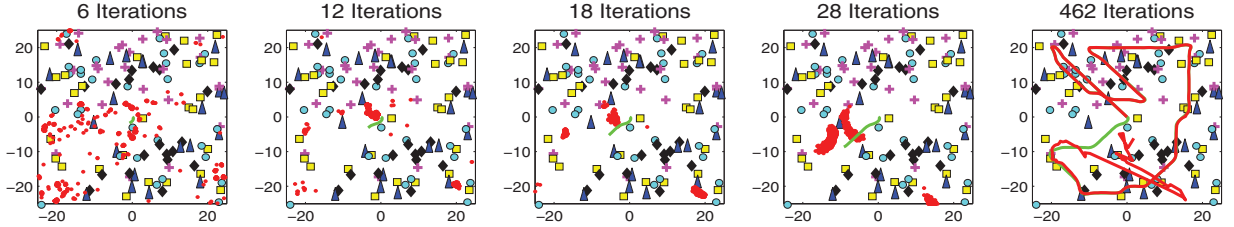


**Fig. 12.** A simulated environment with 45 objects from two classes (yellow squares, blue circles). The plots show the evolution of the particles (red dots), the ground truth trajectory (green), and the estimated trajectory (red). The expected number of clutter detections was set to  $\lambda = 2$ .

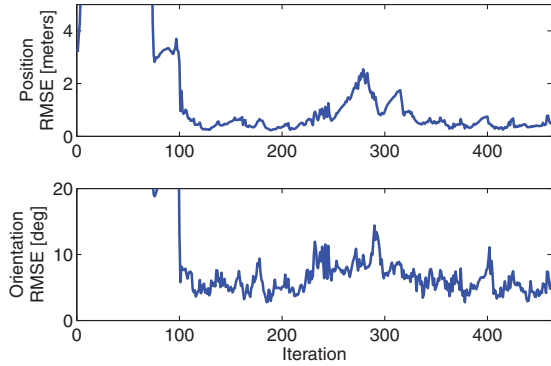


**Fig. 13.** A simulated example of semantic localization in the presence of severe perceptual aliasing. The ground truth trajectory (blue) and the evolution of the particle positions (red points) and orientations (red lines, top left) are shown.

Our semantic localization approach was used to recover the global Tango trajectories in the rest of the runs. Since the prior semantic map contained 2-D object positions, only the horizontal bearing angle was used to update the 2-D position and yaw angle of the phone. A good estimate of the phone's pitch and roll angles can be obtained from the local 6-D trajectory (provided by the Tango phone). Thus, the global semantic localization was performed in 5-D (without the z-axis). This can be extended, of course, if vertical bearing measurements are used and the landmarks in the prior map are annotated with z-coordinates. The active DPM-based detector of Zhu et al. (2014) was used for object recognition. The likelihoods of the semantic observations were computed via the exact permanent algorithm (Algorithm 2). Videos, from two of the experiments, are provided in Extensions 2 and 3. The phone trajectory,

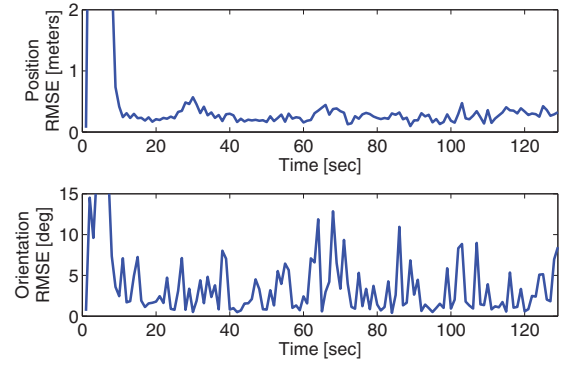


**Fig. 14.** A simulated environment with 150 objects from 5 classes (circles, squares, triangles, crosses, and diamonds) in a  $25 \times 25 \text{ m}^2$  area. The plots show the particles (red dots), the ground truth trajectory (green), and the estimated trajectory (red) for clutter rate  $\lambda = 4$ .

recovered from the second run (Extension 3), is shown in Figure 10. Unfortunately, ground-truth trajectories are not available for these experiments. The videos show 9 global localization trials, in which, on average, 11 sets of semantic observations were needed to obtain an accurate estimate of the phone pose in the prior map. They demonstrate that our algorithm can *repeatedly re-localize* and track the phone pose within the same environment. Moreover, our semantic localization approach is very robust to perceptual aliasing and can improve the visual odometry provided by the phone in ambiguous environments and when closing loops.

### 6.3. Evaluation on the KITTI dataset

This section evaluates the performance of our global semantic localization approach on the KITTI visual

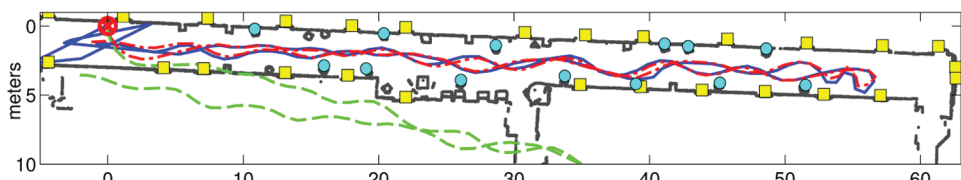
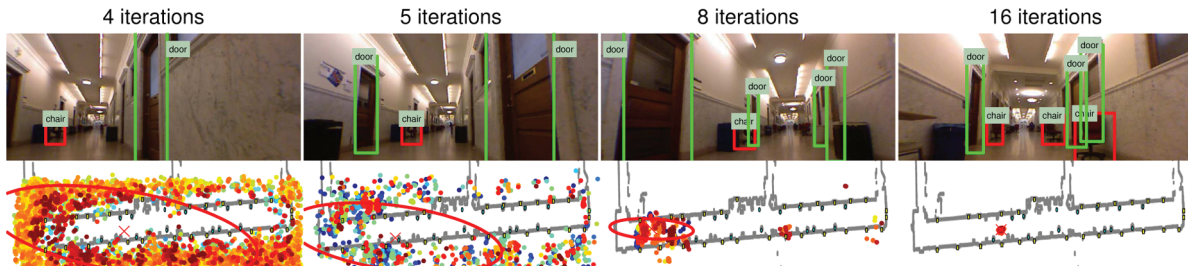


**Fig. 15.** Root-mean-squared error (RMSE) in the pose estimates obtained from the semantic localization algorithm after 50 simulated runs of the scenario in Figure 12.

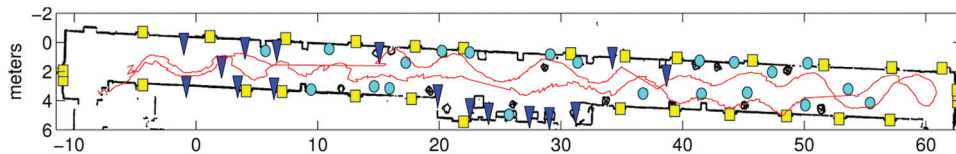
**Table 1.** Comparison of maximum likelihood data association (MLD) and our permanent-based data association approach (PER) with the exact permanent computation (Algorithm 2) on the four robot datasets (Figure 9) and the simulations in Figures 12 and 13. Two types of initializations were used: local (L), for which the initial particle set had errors of up to 1 m and 30°; and global (G), for which the initial particle set was uniformly distributed over the whole environment. Number of particles (NP) in thousands, position error (PE), orientation error (OE), and filter update time (UT), averaged over time, are presented. The first MLD(G) column uses the same number of particles as PER(G), while the second uses a large number in an attempt to improve the performance.

Figure 9	MLD(L)	MLD(G)	MLD(G)	PER(L)	PER(G)
NP [K]	0.50	3.00	40.0	0.50	3.00
PE [m]	0.26	22.9	0.31	0.26	0.26
OE [degrees]	2.54	107	2.75	2.67	2.69
UT [s]	0.023	0.060	0.600	0.065	0.320
Figure 12	MLD(L)	MLD(G)	MLD(G)	PER(L)	PER(G)
NP [K]	0.50	5.00	100	0.50	5.00
PE [m]	15.3	24.9	17.3	0.32	0.72
OE [degrees]	67.0	68.8	72.8	4.58	9.17
UT [s]	0.012	0.062	1.100	0.042	0.400
Figure 13	MLD(L)	MLD(G)	MLD(G)	PER(L)	PER(G)
NP [K]	0.50	24.0	100	0.50	24.0
PE [m]	0.27	48.8	26.9	0.11	2.35
OE [degrees]	3.68	112	74.9	2.08	4.05
UT [s]	0.027	0.760	3.340	0.062	2.620

The reported times are from a MATLAB implementation on a computer with i7 CPU@2.3 GHz and 16 GB RAM. The timing results include only the time needed to perform data association and update the weights for all particles. The time required for object recognition is not included because it is the same for both methods.



**Fig. 16.** Detection score likelihoods obtained from training images.



**Fig. 17.** RMSE between the pose estimates from semantic localization and from lidar-based geometric localization obtained from four real experiments.

odometry dataset (Geiger et al., 2013). The dataset consists of 22 sequences of color stereo images (0.5 megapixels in png format) and 3-D Velodyne point clouds (100,000 points per frame) recorded from a vehicle, driving through residential areas. Eleven sequences (00–10) contain ground-truth vehicle trajectories provided by a GPS/IMU system with real-time kinematic correction. Only sequences {00, 05, 06, 07, 08, 09, 10} were used in

our experiments because the rest either had too few static landmarks or did not contain ground-truth information. The cars (class 1) and windows (class 2) in the RGB image sequences were labeled in order to build prior semantic maps. The Velodyne range information was mapped to the images and the ground-truth trajectories were used to project the labeled objects to the 3-D world coordinate frame. The final semantic maps are provided

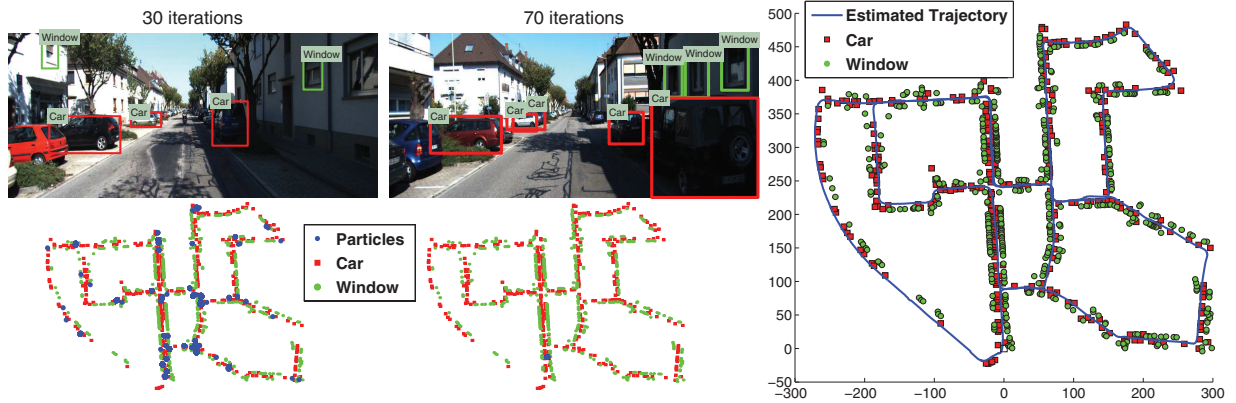


**Fig. 18.** Vehicle trajectory estimated via global semantic localization on sequence 00 from the KITTI visual odometry dataset. The left and middle plots show two images with car and window detections and the corresponding particle distributions in the semantic map. The plot on the right shows the semantic map and the trajectory, recovered after unique localization (iteration 70). See Extensions 5 and 6 for more details.

in Extension 4 and the map for sequence 00 is shown in Figure 18.

The pre-trained deformable-part car models provided in the KITTI object dataset were used for car recognition. Sequence 07 was used to train a deformable-part-model-based window detector and to obtain parameters for the single-object detection model  $p_d(y, x)$ , observation likelihood  $p_z(z|y, x)$ , and clutter model  $p_\kappa(z)$ . The car detection model was nonzero for a distance range of [3, 33] m and used parameters  $p_0 = 0.7$ ,  $m_0 = 11.8$ ,  $v_0 = 14$ . The window detection model was non-zero in the range [7, 24] with parameters  $p_0 = 0.7$ ,  $m_0 = 12.7$ ,  $v_0 = 7$ . The rest of the parameters were:  $p_c(c|y^c) = I_2$ , sensing range 32 m, field of view  $80^\circ$ ,  $\Sigma_\beta = 5^\circ$ , and  $\lambda = 0.5$ .

Visual odometry via Viso2 (Geiger et al., 2011) was used for the prediction step in Algorithm 1. Viso2 provides a 6-D local trajectory. As in the Tango experiments (Section 6.2), only the 2-D position and the yaw angle of the trajectory were updated via our method. The likelihoods of the car-window semantic observations were computed via the exact permanent algorithm (Algorithm 2). Global semantic localization was carried out on sequences 00, 05–10. The vehicle trajectory, recovered from sequence 00, is shown in Figure 18 along with some object detections. A video of the experiment is included in Extension 5. An additional experiment, in which the localization was restarted every 400 iterations, was carried out on sequence 00 and is presented in Extension 6. The experiment demonstrates that our algorithm can repeatedly and successfully re-localize and track the vehicle pose within the same environment. Finally, the results of the global semantic localization on the rest of the sequences (05–10) are presented in Extensions 7–12. The localization errors with respect to the ground-truth trajectories from all experiments are presented in Figure 19. Initially, the errors are large because our method is started with an uninformative prior (a uniform distribution in the area around the landmarks).

Nevertheless, after the initial global localization stage, our approach achieves average errors in the position and orientation estimates of less than 1 m and  $5^\circ$ , respectively. Even though the data association obtained from permanent computations is very robust to perceptual aliasing, sometimes, the ambiguity in the environment is large enough to cause particle depletion problems. For example, if resampling is done too frequently and there is no way to detect if the system is lost (i.e. the particle distribution is never reset), the localization might fail. Such a fail case is shown in Extension 13.

To demonstrate that localization from semantic observations is complementary to existing odometry and SLAM techniques, we also carried out tracking experiments, in which the initial vehicle pose was known. In Figure 20, the position and orientation errors obtained from visual odometry are compared to those obtained from visual odometry, combined with our semantic localization approach. Even though visual odometry provides excellent tracking results by itself, the addition of semantic observations provides a reference to the absolute (semantic map) frame and improves the results.

#### 6.4. Active semantic localization simulations

In this section, we evaluate the performance of the active semantic localization approach (Section 5.1) by comparing it with three other active localization methods in simulation. The simulations use a differential-drive robot model and the motion primitives in Figure 4. Fifty environments of size  $120 \times 120$  m $^2$  containing 300 objects from 3 classes (square, circle, triangle) were generated by sampling random points and placing one of three possible four-object structures (square–square–circle–triangle, square–circle–circle–triangle, or square–triangle–circle–triangle) in order to create perceptual ambiguity (see Figure 21). A start and a goal pose for the robot were chosen in the top-left and

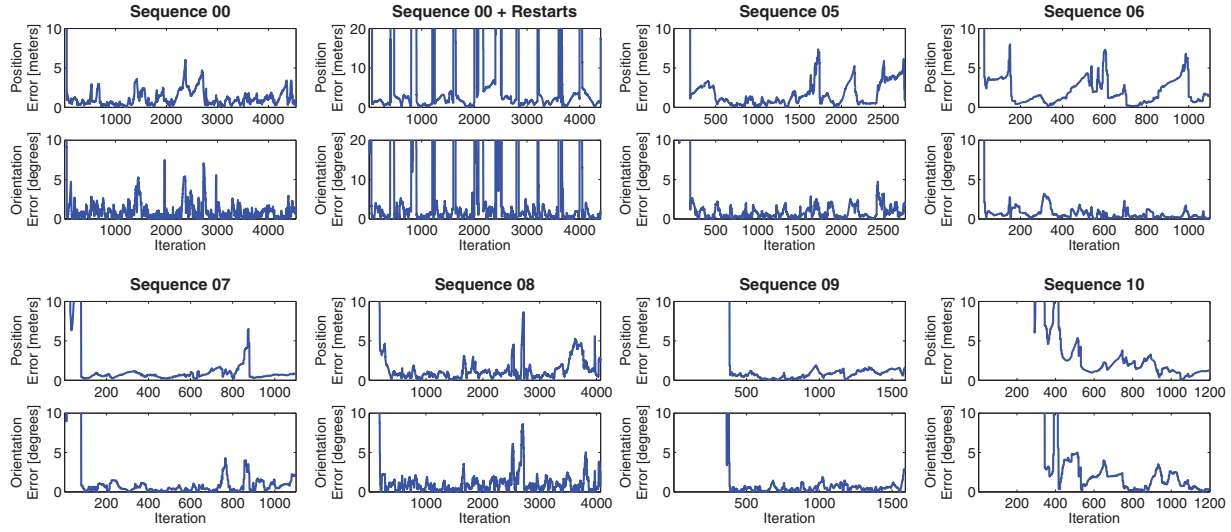


**Fig. 19.** Position (Euclidean distance) and orientation errors of the vehicle trajectories recovered via global semantic localization on sequences {00, 05, 06, 07, 08, 09, 10} from the KITTI visual odometry dataset. The plot, titled “Sequence 00 + Restarts”, shows results from an experiment in which the localization was restarted every 400 iterations. Extensions 5–13 provide videos of all experiments.

**Table 2.** Comparison of the average (over 50 simulated environments) performance of the four active semantic localization approaches, referenced in Figure 21. The average Euclidean distance between the start and the goal positions was 251 m. If the goal was not reached in 1000 iterations, the experiment was terminated. The table presents averages of the number of iterations until termination, the Euclidean distance to the goal at termination, the entropy in the particle distributions, and the position and orientation errors with respect to the ground-truth robot trajectory.

Method	Average number of Steps	Average distance to goal [m]	Average entropy [bits]	Average position error [m]	Average orientation error [deg]
RND	595	35.02	3.00	22.17	12.48
MIN	508	35.58	2.83	27.58	11.98
BEM	447	16.22	3.05	18.49	11.13
ASL	345	12.09	2.05	12.59	6.37

bottom-right corners of each environment, respectively. The semantic localization algorithm (Algorithm 1 with exact permanent computation via Algorithm 2) was initialized with a uniform particle distribution over the whole environment. Semantic observations were simulated using the learned detection, clutter, and measurement likelihood models for cars and windows (from the KITTI dataset in Section 6.3) and red chairs (from the Tango experiments in Section 6.2), corresponding to squares, circles, and triangles, respectively. For each environment, semantic observations were collected, while moving in a straight line, and the filter was updated without resampling until there were 100 effective particles (see Figure 21 for an example of the initial particle set). Starting with this initial particle distribution, the following methods were compared with our active semantic localization approach.

- RND: chooses a motion primitive (from the ones in Figure 4) at random.

- MIN: chooses the motion primitive, which drives the mean of the particle distribution closest to the closest landmark in the environment.
- BEM: chooses a motion primitive by minimizing the entropy of the robot pose conditioned on the future bearing measurements only (see Appendix E for details).

The methods were used to choose motion primitives if the entropy in the particle distribution (computed by discretizing the robot state space into cells of size  $2.5 \times 2.5 \text{ m}^2$  and  $25^\circ$  and replacing the particles, contained in the same cell, with their average) increased above 2.5 bits. Otherwise, if the entropy decreased under 2.5 bits, each method planned a trajectory from the mean of the particle distribution to the goal state using A\* and followed it using a deterministic controller. The trajectories, followed by the four active localization methods, and the associated particle-distribution entropies are shown for one of the

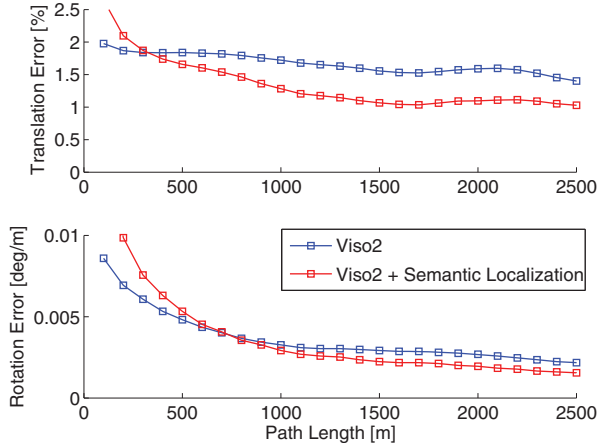


**Fig. 20.** Average translation and orientation errors obtained from visual odometry via Viso2 (Geiger et al., 2011) and from visual odometry combined with semantic localization on sequences {00, 05, 06, 07, 08, 09, 10} from the KITTI visual odometry dataset. Both methods use a known starting vehicle pose, i.e. perform tracking instead of global localization. The orientation error is the cumulative error in degrees between the ground-truth and the estimated orientations divided by path length in meters.

simulated environments in Figure 21. Performance statistics, averaged over the 50 environments, are presented in Table 2. The results show that, on average, our active-semantic-localization approach reaches the goal in less iterations, with lower particle-distribution entropy, and with lower estimation error, compared to the other three approaches. Of course the approach is also a lot more computationally demanding. As expected, the random approach performs the worst because when there no landmarks in proximity to the robot, it might spend a long time until re-

localization. The BEM approach demonstrates much better performance but the main problem with it and the MIN method is that they rely on the mean of the particle distribution for planning. Sometimes, when the mean is far from the true pose, these methods choose trajectories, which do not necessarily result in improved localization accuracy.

## 7. Conclusion

Modeling the semantic information obtained from object recognition with random finite sets enables a unified treatment of data association, missed detections, and clutter. The efficient use of this semantic observation model for Bayesian filtering depends critically on the connection with the matrix permanent. Simulations of our approach showed precise and robust localization from semantic information in various scenarios and over many repetitions. Compared with maximum likelihood data association, our solution is more robust to perceptual aliasing and offers superior performance in cases of global localization and loop-closure. The real experiments demonstrated that the accuracy of the semantic localization method is comparable with the laser-based geometric approaches. More importantly, due to the semantically meaningful observations, our approach is able to repeatedly solve the global localization problem in real environments. Finally, to enable autonomous localization, we addressed the active semantic localization problem, in which the observer's trajectory is selected to minimize the entropy in the pose distribution conditioned on the future semantic measurements. The simulations demonstrated that our method, although computationally demanding, outperforms simpler active localization heuristics. Future work will attempt to replace the particle filter with more sophisticated estimation

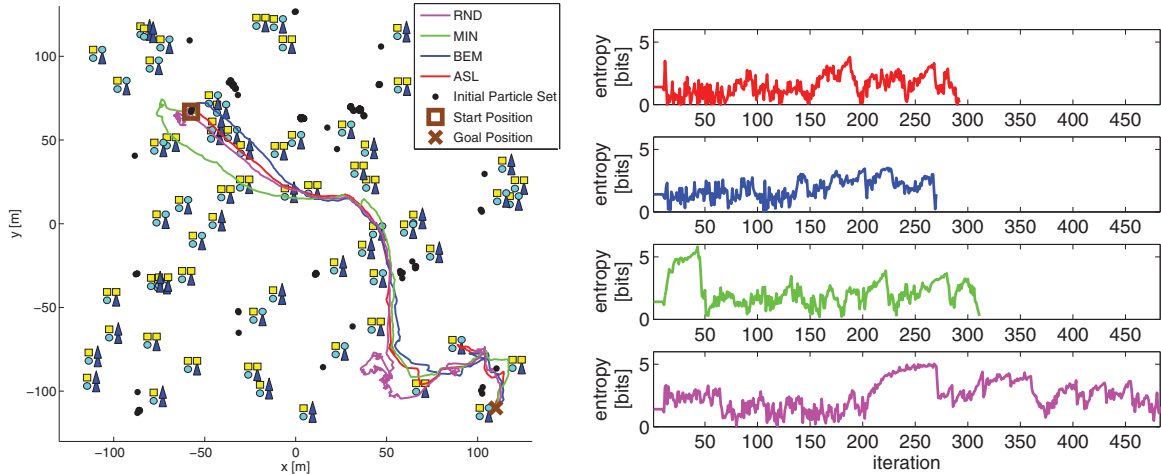


**Fig. 21.** The left plot shows the trajectories, followed by four different active-semantic-localization approaches, which localize and lead a differential-drive robot to a goal pose in a simulated environment containing 300 objects from 3 classes (yellow square, cyan circle, blue triangle). The initial particle distribution is shown by the black dots. The four methods are: (1) ASL, active semantic localization presented in Section 5.1; (2) RND, chooses motion primitives at random; (3) MIN, chooses the motion primitive that drives the particle mean closest to the closest landmark; (4) BEM, bearing-only entropy minimization (see the text for details). The right plot shows the particle-distribution entropies along the trajectories associated with each method.

techniques that handle both discrete (e.g. object classes) and continuous (e.g. object poses) measurements. Examples include inference algorithms for graphical models in the spirit of Kaess et al. (2012) or online optimization techniques such as Jadbabaie et al. (2015). Extensions to semantic mapping and semantic SLAM are of great interest as well.

## Acknowledgements

We thank Chris Clingerman for his help with the MAGIC robot.

## Funding

We gratefully acknowledge support by TerraSwarm, one of six centers of STARNet, a Semiconductor Research Corporation program sponsored by MARCO and DARPA and the following grants: NSF-OIA-1028009, ARL RCTA W911NF-10-2-0016, NSF-DGE-0966142, and NSF-IIS-1317788.

## Notes

1. Visual-odometry and SLAM techniques typically do not use an absolute reference to the world and do not provide global localization. The initial robot pose is chosen as the map origin and is simply tracked over time.
2. See Mahler (2007: Appendix F) for a formal definition of a random finite set
3. For example, in two dimensions, assuming the robot and the sensor frames coincide,  $\beta(x, y) := |\tan^{-1}(x^{p(2)} - y^{p(2)})/(x^{p(1)} - y^{p(1)})| - x^r|$ .
4. The field of view of a camera in two dimensions, assuming its frame coincides with the robot's, can be represented by  $\{w \in \mathbb{R}^2 \mid \|x^p - w\|_2 \leq r_d, \beta(x, w) \leq \alpha_d\}$ , where  $\alpha_d$  is the angle of view and  $r_d$  is the maximum range at which an object can be detected.
5. It is possible to track the data association distribution over time (see Bar-Shalom et al. (2009)).
6. A matching in graph  $G$  is a subgraph of  $G$  in which no two edges share a common vertex. The weight of a matching is the product of all of its edge weights. A matching is perfect if it contains all of  $G$ 's vertices.
7. A #P-complete problem is equivalent to computing the number of accepting paths of a polynomial-time nondeterministic Turing machine and #P contains NP.

## References

- Anati R, Scaramuzza D, Derpanis K and Daniilidis K (2012) Robot localization using soft object detection. In: *IEEE international conference on robotics and automation (ICRA)*, pp. 4992–4999.
- Angeli A, Doncieux S, Meyer J and Filliat D (2009) Visual topological SLAM and global localization. In: *IEEE international conference on robotics and automation (ICRA)*.
- Atanasov N, Le Ny J, Daniilidis K and Pappas G (2015) Decentralized active information acquisition: theory and application to multi-robot SLAM. In: *IEEE international conference on robotics and automation (ICRA)*.
- Atanasov N, Zhu M, Daniilidis K and Pappas G (2014) Semantic localization via the matrix permanent. In: *Robotics: science and systems (RSS)*, pp. 1–10. Available at: <http://www.roboticsproceedings.org/rss10/p43.html>
- Bailey T (2002) *Mobile Robot Localisation and Mapping in Extensive Outdoor Environments*. Dissertation, The University of Sydney.
- Bao S and Savarese S (2011) Semantic structure from motion. In: *Computer vision and pattern recognition (CVPR)*.
- Bar-Shalom Y, Daum F and Huang J (2009) The probabilistic data association filter. *IEEE Control Systems* 29(6): 82–100.
- Bezáková I, Štefankovič D, Vazirani V and Vigoda E (2006) Accelerating simulated annealing for the permanent and combinatorial counting problems. In: *ACM-SIAM symposium on discrete algorithms*, pp. 900–907.
- Bishop A and Jensfelt P (2010) Global robot localization with random finite set statistics. In: *International conference on information fusion*.
- Charrow B, Kumar V and Michael N (2013) Approximate representations for multi-robot control policies that maximize mutual information. In: *Proceedings of robotics: science and systems (RSS)*, pp. 1–8.
- Civera J, Galvez-Lopez D, Riazuelo L, Tardos J and Montiel J (2011) Towards semantic SLAM using a monocular camera. In: *IEEE/RSJ international conference on intelligent robots and systems (IROS)*, pp. 1277–1284.
- Collins J and Uhlmann J (1992) Efficient gating in data association with multivariate Gaussian distributed states. *IEEE Transactions on Aerospace and Electronic Systems* 28(3): 909–916.
- Cover T and Thomas J (2006) *Elements of Information Theory*. 2nd edn. New York: Wiley-Interscience.
- Cummins M and Newman P (2008) FAB-MAP: Probabilistic Localization and Mapping in the Space of Appearance. *The International Journal of Robotics Research* 27(6): 647–665.
- Dame A, Prisacariu V, Ren C and Reid I (2013) Dense reconstruction using 3D object shape priors. In: *Computer vision and pattern recognition (CVPR)*.
- Dames P, Thakur D, Schwager M and Kumar V (2013) Playing fetch with your robot: the ability of robots to locate and interact with objects. *IEEE Robotics and Automation Magazine* 21(2): 46–52.
- Dellaert F, Fox D, Burgard W and Thrun S (1999) Monte Carlo localization for mobile robots. In: *IEEE international conference on robotics and automation (ICRA)*, vol. 2, pp. 1322–1328.
- Felzenszwalb P, Girshick R, McAllester D and Ramanan D (2010) Object detection with discriminatively trained part-based models. *IEEE Transactions on Pattern Analysis and Machine Intelligence* 32(9): 1627–1645.
- Fox D, Burgard W and Thrun S (1998) Active Markov localization for mobile robots. *Robotics and Autonomous Systems* 25: 195–207.
- Galindo C, Saffiotti A, Coradeschi S, Buschka P, Fernandez-Madrigal J and Gonzalez J (2005) Multi-hierarchical semantic maps for mobile robotics. In: *IEEE/RSJ international conference on intelligent robots and systems (IROS)*, pp. 2278–2283.
- Geiger A, Lenz P, Stiller C and Urtasun R (2013) Vision meets robotics: the KITTI Dataset. *The International Journal of Robotics Research* 32(11): 1231–1237.
- Geiger A, Ziegler J and Stiller C (2011) StereoScan: dense 3D reconstruction in real-time. In: *Intelligent vehicles symposium (IV)*, pp. 963–968.
- Google ATAP group (2014) Project Tango. <https://www.google.com/atap/projecttango>.
- Hesch J, Kottas D, Bowman S and Roumeliotis S (2013) Towards consistent vision-aided inertial navigation. In: *Algorithmic*

- Foundations of Robotics X* (Springer Tracts in Advanced Robotics, vol. 86). New York: Springer.
- Howard A and Gerkey B (2002) Adaptive Monte-Carlo Localization (AMCL) package. Robot Operating System (ROS), available at: <http://wiki.ros.org/amcl>.
- Jadbabaie A, Rakhlin A, Shahrampour S and Sridharan K (2015) Online optimization: competing with dynamic comparators. In: *International conference on artificial intelligence and statistics (AISTATS)*, pp. 398–406.
- Jerrum M, Sinclair A and Vigoda E (2004) A polynomial-time approximation algorithm for the permanent of a matrix with nonnegative entries. *Journal of the ACM* 51(4): 671–697.
- Kaess M, Johannsson H, Roberts R, Ila V, Leonard J and Dellaert F (2012) iSAM2: incremental smoothing and mapping using the Bayes tree. *The International Journal of Robotics Research* 31(2): 216–235.
- Kaess M, Ranganathan A and Dellaert F (2008) iSAM: incremental smoothing and mapping. *IEEE Transactions on Robotics (TRO)* 24(6): 1365–1378.
- Kalyan B, Lee K and Wijesoma W (2010) FISST-SLAM: finite set statistical approach to simultaneous localization and mapping. *The International Journal of Robotics Research* 29(10): 1251–1262.
- Karasev V, Chiuso A and Soatto S (2012) Controlled recognition bounds for visual learning and exploration. In: *Advances in Neural Information Processing Systems (NIPS)*.
- Ko D, Yi C and Suh I (2013) Semantic mapping and navigation: a Bayesian approach. In: *IEEE/RSJ international conference on intelligent robots and systems (IROS)*, pp. 2630–2636.
- Košecká J and Li F (2004) Vision based topological Markov localization. In: *IEEE international conference on robotics and automation (ICRA)*, vol. 2, pp. 1481–1486.
- Kostavelis I and Gasteratos A (2013) Learning Spatially Semantic Representations for Cognitive Robot Navigation. *Robotics and Autonomous Systems* 61(12): 1460–1475.
- Kummerle R, Grisetti G, Strasdat H, Konolige K and Burgard W (2011)  $g^2o$ : a general framework for graph optimization. In: *IEEE international conference on robotics and automation (ICRA)*, pp. 3607–3613.
- Law W (2009) *Approximately Counting Perfect and General Matchings in Bipartite and General Graphs*. Dissertation, Duke University.
- Lee C, Clark D and Salvi J (2013) SLAM with dynamic targets via single-cluster PHD filtering. *IEEE Journal of Selected Topics in Signal Processing* 7(3): 543–552.
- Liggins M, Hall D and Llinas J (2008) *Handbook of Multisensor Data Fusion*. London: Taylor & Francis.
- Ma WK, Vo BN, Singh S and Baddeley A (2006) Tracking an unknown time-varying number of speakers using TDOA measurements: a random finite set approach. *IEEE Transactions on Signal Processing* 54(9): 3291–3304.
- Mahler R (2007) *Statistical Multisource-Multitarget Information Fusion*. Artech House.
- Mariottini G and Roumeliotis S (2011) Active vision-based robot localization and navigation in a visual memory. In: *IEEE international conference on robotics and automation (ICRA)*.
- Montemerlo M and Thrun S (2003) Simultaneous localization and mapping with unknown data association using FastSLAM. In: *IEEE international conference on robotics and automation (ICRA)*, vol. 2, pp. 1985–1991.
- Morelande M (2009) Joint data association using importance sampling. In: *International conference on information fusion*, pp. 292–299.
- Mullane J, Vo BN, Adams M and Vo BT (2011) *Random Finite Sets for Robot Mapping & SLAM* (Springer Tracts in Advanced Robotics). New York: Springer.
- Nijenhuis A and Wilf H (1978) *Combinatorial Algorithms*. New York: Academic Press.
- Nüchter A and Hertzberg J (2008) Towards semantic maps for mobile robots. *Robotics and Autonomous Systems* 56(11): 915–926.
- Oh S, Russell S and Sastry S (2009) Markov chain Monte Carlo data association for multi-target tracking. *IEEE Transactions on Automatic Control* 54(3): 481–497.
- Pasula H, Russell S, Ostland M and Ritov Y (1999) Tracking many objects with many sensors. In: *Proceedings of the international joint conference on artificial intelligence (IJCAI)*, vol. 2, pp. 1160–1167.
- Pronobis A (2011) *Semantic Mapping with Mobile Robots*. PhD Dissertation, KTH Royal Institute of Technology. Available at: <http://www.pronobis.pro/phd>.
- Ryser H (1963) *Combinatorial Mathematics* (Carus Mathematical Monographs, no. 14). Mathematical Association of America.
- Se S, Lowe D and Little J (2005) Vision-based global localization and mapping for mobile robots. *IEEE Transactions on Robotics* 21(3): 364–375.
- Sidenbladh H and Wirkander SL (2003) Tracking random sets of vehicles in terrain. In: *Computer vision and pattern recognition workshop*, vol. 9, p. 98.
- Sünderhauf N and Protzel P (2011) BRIEF-Gist - closing the loop by simple means. In: *IEEE/RSJ international conference on intelligent robots and systems (IROS)*, pp. 1234–1241.
- Thrun S, Burgard W and Fox D (2005) *Probabilistic Robotics*. Cambridge, MA: MIT Press.
- Valiant L (1979) The complexity of computing the permanent. *Theoretical Computer Science* 8(2): 189–1201.
- Wang J, Zha H and Cipolla R (2006) Coarse-to-fine vision-based localization by indexing scale-invariant features. *IEEE Transactions on Systems, Man, and Cybernetics* 36(2): 413–422.
- Wolf J, Burgard W and Burkhardt H (2005) Robust vision-based localization by combining an image retrieval system with Monte Carlo localization. *IEEE Transactions on Robotics* 21(2): 208–216.
- Wong L, Kaelbling L and Lozano-Pérez T (2013) Data association for semantic world modeling from partial views. In: *International symposium on robotics research (ISRR)*. Available at: <http://people.csail.mit.edu/lsw/research.html>
- Yi C, Suh IH, Lim GH and Choi BU (2009) Active–semantic localization with a single consumer-grade camera. In: *IEEE International conference on systems, man and cybernetics*, pp. 2161–2166.
- Zhang F, Stahle H, Gaschler A, Buckl C and Knoll A (2012) Single camera visual odometry based on random finite set statistics. In: *IEEE/RSJ international conference on intelligent robots and systems (IROS)*, pp. 559–566.
- Zhu M, Atanasov N, Pappas G and Daniilidis K (2014) Active deformable part models inference. In: *European conference on computer vision (ECCV)*, pp. 281–296.

## Appendix A: Index to Multimedia Extensions

Archives of IJRR multimedia extensions published prior to 2014 can be found at <http://www.ijrr.org>, after 2014 all videos are available on the IJRR YouTube channel at <http://www.youtube.com/user/ijrrmultimedia>

**Table of Multimedia Extensions**

Extension	Media type	Description
1	Video	Mobile robot localization from semantic observations
2	Video	Global positioning of the Tango phone
3	Video	Global positioning of the Tango phone
4	Data	Car and window positions used for the semantic maps in the KITTI dataset experiments
5	Video	Global semantic localization on KITTI dataset sequence 00
6	Video	Global semantic localization on KITTI dataset sequence 00 with several restarts
7	Video	Global semantic localization on KITTI dataset sequence 05
8	Video	Global semantic localization on KITTI dataset sequence 06
9	Video	Global semantic localization on KITTI dataset sequence 07
10	Video	Global semantic localization on KITTI dataset sequence 08
11	Video	Global semantic localization on KITTI dataset sequence 09
12	Video	Global semantic localization on KITTI dataset sequence 10
13	Video	Global semantic localization on KITTI dataset sequence 08 (fail case)

## Appendix B: Validity of the data association pdfs

For simplicity, let  $p_d(y_i, x) = p_d(y_j, x) \equiv p_d$  for all  $i, j$  in this section. We verify that  $p(\pi|Y_d(x), x)$  is a valid pdf in each of the following cases.

### B.1. No missed detections and no false positives

In this case,  $\pi \in \Pi_{n,n}$  with likelihood  $p(\pi|Y_d(x), x) = 1/n!$ , which sums to one as follows:

$$\sum_{\pi \in \Pi_{n,n}} p(\pi|Y_d(x), x) = \frac{1}{n!} |\Pi_{n,n}| = 1$$

### B.2. No false positives but missed detections are possible

In this case,  $\pi \in \Pi_{m,n}$  with likelihood:

$$p(\pi|Y_d(x), x) = \frac{1}{m!} p_d^m (1 - p_d)^{n-m}$$

which sums to one using the binomial theorem:

$$\begin{aligned} \sum_{m=0}^n \sum_{\pi \in \Pi_{m,n}} p(\pi|Y_d(x), x) &= \sum_{m=0}^n {}_n P_m \frac{1}{m!} p_d^m (1 - p_d)^{n-m} \\ &= (p_d + (1 - p_d))^n = 1 \end{aligned}$$

### B.3. No missed detections but false positives are possible

In this case,  $\pi \in \Pi_{n,m}$  with likelihood:

$$p(\pi|Y_d(x), x) = \frac{1}{m P_n} \frac{e^{-\lambda} \lambda^{m-n}}{(m-n)!}$$

which sums to one as follows:

$$\sum_{m=n}^{\infty} \sum_{\pi \in \Pi_{n,m}} p(\pi|Y_d(x), x) = \sum_{m=n}^{\infty} {}_m P_n \frac{1}{m P_n} \frac{e^{-\lambda} \lambda^{m-n}}{(m-n)!} = 1$$

### B.4. Both missed detections and false positives are possible

The likelihood of  $\pi \in \bar{\Pi}_{n,m}$  with  $k$  true positive assignments is

$$p(\pi|Y_d(x), x) = \frac{1}{m P_k} p_d^k (1 - p_d)^{n-k} \frac{e^{-\lambda} \lambda^{m-k}}{(m-k)!}$$

which sums to one as follows:

$$\begin{aligned} &\sum_{m=0}^{\infty} \sum_{k=0}^{\min\{m,n\}} \binom{n}{k} {}_m P_k p(\pi|Y_d(x), x) \\ &= \sum_{m=0}^{\infty} \sum_{k=0}^{\min\{m,n\}} \binom{n}{k} p_d^k (1 - p_d)^{n-k} \frac{e^{-\lambda} \lambda^{m-k}}{(m-k)!} \\ &= \sum_{m=0}^n \sum_{k=0}^m \binom{n}{k} p_d^k (1 - p_d)^{n-k} \frac{e^{-\lambda} \lambda^{m-k}}{(m-k)!} \\ &+ \sum_{m=n+1}^{\infty} \sum_{k=0}^n \binom{n}{k} p_d^k (1 - p_d)^{n-k} \frac{e^{-\lambda} \lambda^{m-k}}{(m-k)!} \\ &\stackrel{\text{switch index order}}{=} \sum_{k=0}^n \sum_{m=k}^n \binom{n}{k} p_d^k (1 - p_d)^{n-k} \frac{e^{-\lambda} \lambda^{m-k}}{(m-k)!} \\ &+ \sum_{k=0}^n \sum_{m=n+1}^{\infty} \binom{n}{k} p_d^k (1 - p_d)^{n-k} \frac{e^{-\lambda} \lambda^{m-k}}{(m-k)!} \\ &= \sum_{k=0}^n \binom{n}{k} p_d^k (1 - p_d)^{n-k} \left[ \sum_{m=k}^{\infty} \frac{e^{-\lambda} \lambda^{m-k}}{(m-k)!} \right] = 1 \end{aligned}$$

## Appendix C: Proof of Theorem 1

Let  $V_1 := Y_d(x)$  and  $V_2 := Z$  be the vertices of a weighted complete bipartite graph  $G := (V_1, V_2, E, w)$ , where the weight  $w_e$  associated with  $e := (i, j) \in E$  is  $Q(i, j)$ . The functions  $\pi$  in (9) specify different data associations between the objects  $V_1$  and the measurements  $V_2$ . The introduction of missed detections (“0” in the range of  $\pi$ ) means that some detectable objects need not to be assigned to a measurement in  $Z$ . As any object could be missed, the data associations  $\pi$  correspond to *matchings* (not necessarily perfect as before) in the graph  $G$ . Given a matching  $\pi$ , the associated product term inside the sum in (9) corresponds to the weight of  $\pi$ . The sum over all  $\pi$  corresponds to the sum of the weights of all matchings in  $G$ . The sum of the weights of all  $k$ -matchings (matchings with  $k$  edges) can be computed via the  $k$ th subpermanent sum of the adjacency matrix  $Q$  of  $G$ .

**Definition 2** (Subpermanent sum). *Let  $A$  be an  $n \times m$  non-negative matrix with  $n \leq m$  and let  $Q_{k,n}$  be the set of all subsets of cardinality  $k$  of  $1, \dots, n$ . For  $\alpha \in Q_{k,n}$  and  $\beta \in Q_{k,m}$  let  $A[\alpha, \beta] := [A(\alpha_i, \beta_j)]_{i,j=1}^k$  be the corresponding  $k \times k$  submatrix of  $A$ . Define  $\text{per}_0(A) := 1$  and*

$$\text{per}_k(A) := \sum_{\alpha \in Q_{k,n}, \beta \in Q_{k,m}} \text{per}(A[\alpha, \beta]), \quad k = 1, \dots, n$$

Then, the sum in (9) is equal to the sum over the weights of all  $k$ -matchings:

$$\sum_{\pi} \prod_{i|\pi(i)>0} \frac{p_d(y_i, x)p_z(z_{\pi(i)}|y_i, x)}{(1 - p_d(y_i, x))\lambda p_k(z_{\pi(i)})} = \sum_{k=0}^{|Y_d(x)|} \text{per}_k(Q) \quad (19)$$

where the assumption that  $|Y_d(x)| \leq m$  is used. The following two lemmas describe a reduction from the problem of summing all subpermanent sums of a rectangular matrix (or matchings in an unbalanced bipartite graph) to the problem of the permanent of a rectangular matrix (or perfect matchings in an unbalanced bipartite graph) and then to the problem of the permanent of a square matrix (or perfect matchings in a balanced bipartite graph).

**Lemma 1.** *Let  $A_{n,m}$  be an  $n \times m$  matrix with  $n \leq m$ . Then,*

$$\sum_{k=0}^n \text{per}_k(A_{n,m}) = \text{per}([A_{n,m} \ I_n])$$

*Proof.* Associate  $A$  with a weighted complete bipartite graph  $G_A := (V_1 := \{1, \dots, n\}, V_2 := \{1, \dots, m\}, E, w_A)$ , where the weights  $w_A$  corresponding with the entries of  $A$ . To obtain the graph  $G_B$  associated with  $B := [A_{n,m} \ I_n]$  add  $n$  dummy nodes  $V_3$  to  $V_2$  and  $n$  edges of weight 1. For

$k \in \{0, \dots, n\}$ , fix subsets  $\alpha \in Q_{k,n}$  and  $\beta \in Q_{k,m}$  using the notation from Definition 2. A perfect matching in  $G_B$  associated with  $\alpha$  and  $\beta$  corresponds to:

- a  $k$ -matching between  $\alpha \in V_1$  and  $\beta \in V_2$  of weight  $\text{per}(A[\alpha, \beta])$ ;
- a  $(n - k)$ -matching between  $V_1 \setminus \alpha$  and  $V_3$  of weight 1.

Then,  $\text{per}(B)$  is the sum of all perfect matchings in  $G_B$ :

$$\text{per}(B) = \sum_{k=0}^n \sum_{\substack{\beta \in Q_{k,m} \\ \alpha \in Q_{k,n}}} \text{per}(A[\alpha, \beta]) = \sum_{k=0}^n \text{per}_k(A)$$

where the last equality follows directly from Definition 2.

**Lemma 2.** *Let  $A_{n,m}$  be an  $n \times m$  matrix with  $n \leq m$ . Then,*

$$\text{per}(A_{n,m}) = \frac{1}{(m-n)!} \text{per}\left(\begin{bmatrix} A_{n,m} \\ 1_{m-n,m} \end{bmatrix}\right)$$

where  $1_{m-n,m}$  is a  $(m - n) \times m$  matrix of all ones.

*Proof.* Associate  $A$  with a weighted complete bipartite graph  $G_A := (V_1 := \{1, \dots, n\}, V_2 := \{1, \dots, m\}, E, w_A)$ , where the weights  $w_A$  correspond with the entries of  $A$ . To obtain the graph  $G_B$  associated with  $B := [A_{n,m}^T \ 1_{m-n,m}^T]^T$  dummy nodes  $V_3$  to  $V_1$  and  $(m - n)m$  edges of weight 1. Fix a subset  $\beta \in Q_{m-n,m}$  using the notation from Definition 2. A perfect matching in  $G_B$  associated with  $\beta$  corresponds to:

- a  $n$ -matching between  $V_1$  and  $V_2 \setminus \beta$  of weight  $\text{per}(A[V_1, V_2 \setminus \beta])$ ;
- a  $(m - n)$ -matching between  $V_3$  and  $\beta$  of weight  $(m - n)!$ .

Then,  $\text{per}(B)$  is the sum of all perfect matchings in  $G_B$ :

$$\begin{aligned} \text{per}(B) &= \sum_{\beta \in Q_{m-n,m}} (m - n)! \text{per}(A[V_1, V_2 \setminus \beta]) \\ &= (m - n)! \text{per}(A) \end{aligned}$$

where the last equality follows directly from Definition 2.

The proof is completed by combining the two reductions above to write the sum in (19) as

$$\sum_{k=0}^{|Y_d(x)|} \text{per}_k(Q) = \frac{1}{m!} \text{per}\left(\begin{bmatrix} Q & I_{|Y_d(x)|} \\ 1_{m,m} & 1_{m,|Y_d(x)|} \end{bmatrix}\right)$$

**Table 3.** *No missed detections and no clutter:* the likelihood  $p(Z|Y_d(x), x)$  of a set of semantic observations  $Z$  is shown for different combinations of  $m := |Z|$  and  $n := |Y_d(x)|$ . The dependence of the likelihoods on  $x$  is omitted for clarity.

$n \neq m$	0
$0 = m = n$	1
$0 < m = n$	$\frac{1}{m!} \text{per} \begin{bmatrix} p_z(z_1 y_1) & \cdots & p_z(z_m y_1) \\ \vdots & & \vdots \\ p_z(z_1 y_n) & \cdots & p_z(z_m y_n) \end{bmatrix}$

**Table 4.** *No clutter but missed detections are possible:* the likelihood  $p(Z|Y_d(x), x)$  of a set of semantic observations  $Z$  is shown for different combinations of  $m := |Z|$  and  $n := |Y_d(x)|$ . The dependence of the likelihoods on  $x$  is omitted for clarity.

$n < m$	0
$0 = m \leq n$	$\prod_{i=1}^n (1 - p_d(y_i))$
$0 < m \leq n$	$\frac{1}{m!(n-m)!} \text{per} \begin{bmatrix} p_d(y_1)p_z(z_1 y_1) & \cdots & p_d(y_1)p_z(z_m y_1) & 1 - p_d(y_1) & \cdots & 1 - p_d(y_1) \\ \vdots & & \vdots & \vdots & & \vdots \\ p_d(y_n)p_z(z_1 y_n) & \cdots & p_d(y_n)p_z(z_m y_n) & 1 - p_d(y_n) & \cdots & 1 - p_d(y_n) \end{bmatrix}$

**Table 5.** *No missed detections but clutter is possible:* the likelihood  $p(Z|Y_d(x), x)$  of a set of semantic observations  $Z$  is shown for different combinations of  $m := |Z|$  and  $n := |Y_d(x)|$ . The dependence of the likelihoods on  $x$  is omitted for clarity.

$m < n$	0
$0 = n \leq m$	$\frac{e^{-\lambda} \lambda^m}{m!} \prod_{j=1}^m p_\kappa(z_j) \text{per} \begin{bmatrix} p_z(z_1 y_1) & \cdots & p_z(z_m y_1) \\ \vdots & & \vdots \\ p_z(z_1 y_n) & \cdots & p_z(z_m y_n) \\ \lambda p_\kappa(z_1) & \cdots & \lambda p_\kappa(z_m) \\ \vdots & & \vdots \\ \lambda p_\kappa(z_1) & \cdots & \lambda p_\kappa(z_m) \end{bmatrix}$
$0 < n \leq m$	$\frac{e^{-\lambda}}{m!(m-n)!} \text{per} \begin{bmatrix} p_z(z_1 y_1) & \cdots & p_z(z_m y_1) \\ \vdots & & \vdots \\ p_z(z_1 y_n) & \cdots & p_z(z_m y_n) \\ \lambda p_\kappa(z_1) & \cdots & \lambda p_\kappa(z_m) \\ \vdots & & \vdots \\ \lambda p_\kappa(z_1) & \cdots & \lambda p_\kappa(z_m) \end{bmatrix}$

## Appendix D: Summary of the semantic observation models

Tables 3–6 provide a summary of the semantic observation models.

## Appendix E: Active bearing-only localization

Finally, we present details about the bearing-only entropy minimization (BEM) method. It solves the active semantic localization problem in (12) but the pose entropy is conditioned only on the future bearing measurements:

$$\begin{aligned} \sigma^* \in \arg \min_{\sigma \in \Sigma} \quad & \mathbb{H}(x_{0:T}|B_{1:T}) \\ \text{subject to} \quad & x_{s+1} = f(x_s, \sigma_s, v_s), \quad s = 0, \dots, T-1 \\ & B_s = \{\beta(x_s, y) + \eta_s | y^p \in \text{FoV}(x_s)\}, \quad s = 1, \dots, T \end{aligned} \quad (20)$$

where  $\eta_s \sim \mathcal{N}(0, \Sigma_\beta)$  is the bearing-measurement noise and  $B_s$  is the set of bearing measurements obtained at time  $s$ . Since the robot motion model  $f(x, u, v)$  and the bearing measurement model  $\beta(x, y)$  are continuous functions of the robot state  $x$  and landmark states  $y$ , perturbed by Gaussian noise, we can linearize them to simplify the above problem. In detail, let  $\bar{x}_s$  be the mean of the particle distribution at time  $s$  and define  $\delta x_s := x_s - \bar{x}_s$ . We linearize the constraints in Problem (20) around the means  $\bar{x}_s$  and  $\beta(\bar{x}_s, y)$  to obtain

$$\begin{aligned} \sigma^* \in \arg \min_{\sigma \in \Sigma} \quad & \mathbb{H}(\delta x_{0:T}) - \mathbb{I}(\delta x_{0:T}; \delta B_{1:T}) \\ \text{subject to} \quad & \bar{x}_{s+1} = f(\bar{x}_s, \sigma_s, 0), \quad s = 0, \dots, T-1 \\ & \delta x_s \approx \left[ \frac{\partial f}{\partial x}(\bar{x}_s, \sigma_s, 0) \right] \delta x_s + \left[ \frac{\partial f}{\partial v}(\bar{x}_s, \sigma_s, 0) \right] v_s \\ & \delta B_s \approx \left\{ \frac{\partial \beta}{\partial x}(\bar{x}_s, y) \delta x_s + \eta_s | y^p \in \text{FoV}(x_s) \right\}, \quad s = 1, \dots, T \end{aligned} \quad (21)$$

**Table 6.** Both missed detections and clutter are possible: the likelihood  $p(Z|Y_d(x), x)$  of a set of semantic observations  $Z$  is shown for different combinations of  $m := |Z|$  and  $n := |Y_d(x)|$ . The dependence of the likelihoods on  $x$  is omitted for clarity.

$n = 0$	$\frac{e^{-\lambda}}{m!} \prod_{j=1}^m p_\kappa(z_j)$
$m = 0$	$\prod_{i=1}^n (1 - p_d(y_i))$
$0 < n \leq m$	$\frac{e^{-\lambda}}{m!n!} \text{per} \begin{bmatrix} \frac{p_d(y_1)p_z(z_1 y_1)}{\lambda p_\kappa(z_1)} & \dots & \frac{p_d(y_1)p_z(z_m y_1)}{\lambda p_\kappa(z_m)} & 1 - p_d(y_1) & 0 \\ \vdots & & \vdots & & \ddots \\ \frac{p_d(y_n)p_z(z_1 y_n)}{\lambda p_\kappa(z_1)} & \dots & \frac{p_d(y_n)p_z(z_m y_n)}{\lambda p_\kappa(z_m)} & 0 & 1 - p_d(y_n) \\ \lambda p_\kappa(z_1) & \dots & \dots & \dots & \lambda p_\kappa(z_1) \\ \vdots & & & & \vdots \\ \lambda p_\kappa(z_m) & \dots & \dots & \dots & \lambda p_\kappa(z_m) \\ \frac{p_d(y_1)p_z(z_1 y_1)}{\lambda p_\kappa(z_1)} & \dots & \frac{p_d(y_1)p_z(z_m y_1)}{\lambda p_\kappa(z_m)} & 1 - p_d(y_1) & \dots & 1 - p_d(y_1) \\ \vdots & & \vdots & & \vdots & \vdots \\ \frac{p_d(y_n)p_z(z_1 y_n)}{\lambda p_\kappa(z_1)} & \dots & \frac{p_d(y_n)p_z(z_m y_n)}{\lambda p_\kappa(z_m)} & 1 - p_d(y_n) & \dots & 1 - p_d(y_n) \\ \lambda p_\kappa(z_1) & \dots & 0 & \lambda p_\kappa(z_1) & \dots & \lambda p_\kappa(z_1) \\ \vdots & & & \vdots & & \vdots \\ 0 & & \lambda p_\kappa(z_m) & \lambda p_\kappa(z_m) & \dots & \lambda p_\kappa(z_m) \end{bmatrix}$
$0 < m \leq n$	$\frac{e^{-\lambda}}{m!n!} \text{per} \begin{bmatrix} \frac{p_d(y_1)p_z(z_1 y_1)}{\lambda p_\kappa(z_1)} & \dots & \frac{p_d(y_1)p_z(z_m y_1)}{\lambda p_\kappa(z_m)} & 1 - p_d(y_1) & \dots & 1 - p_d(y_1) \\ \vdots & & \vdots & & \vdots & \vdots \\ \frac{p_d(y_n)p_z(z_1 y_n)}{\lambda p_\kappa(z_1)} & \dots & \frac{p_d(y_n)p_z(z_m y_n)}{\lambda p_\kappa(z_m)} & 1 - p_d(y_n) & \dots & 1 - p_d(y_n) \\ \lambda p_\kappa(z_1) & \dots & 0 & \lambda p_\kappa(z_1) & \dots & \lambda p_\kappa(z_1) \\ \vdots & & & \vdots & & \vdots \\ 0 & & \lambda p_\kappa(z_m) & \lambda p_\kappa(z_m) & \dots & \lambda p_\kappa(z_m) \end{bmatrix}$

Let  $C_0$  be the covariance of the prior particle distribution and assume that  $\delta x_0 \sim \mathcal{N}(0, C_0)$ . Since the constraints in (21) are linear and the measurement noise is Gaussian, the distribution of  $\delta x_s$  remains Gaussian for  $s = 1, \dots, T$ . In particular, it can be computed via the Kalman filter. In addition, the entropy and mutual information of Gaussian random variables depend only on the associated covariance

matrices (and not on the particular measurement realization  $\delta B_{1:T}$ ) and can be computed in closed form. Thus, we compute the cost for each control sequence  $\sigma \in \Sigma$  and choose the sequence with the lowest cost. Refer to Atanasov et al. (2015) for more details regarding conditional entropy minimization via linearization and model predictive control.